FREQUENCY RESPONSE TECHNIQUES FOR THE CHARACTERIZATION OF POROUS CATALYTIC SOLIDS

Sebastian C. Reyes and Enrique Iglesia*
Corporate Research Laboratories
Exxon Research and Engineering Company
Annandale, NJ 08801

* Current Address: Department of Chemical Engineering
University of California at Berkeley
Berkeley, CA 94720

in Catalysis, Specialist Periodical Reports, (Spivey, J.J., ed.) Vol. 11, p.51. Royal Society of Chemistry, Thomas Graham House, Cambridge, UK, 1994.

OUTLINE

1. Introduction

1.1 Transient Methods

The response of a dynamic system to a sudden change in concentration or temperature yields kinetic information on the rate of chemical and physical processes occurring within the perturbed volume. When amplitude changes are small, or when only the isotopic composition is changed, the system remains at quasisteady-state and the mechanisms of chemical or transport processes are unaffected by the imposed perturbation. Small perturbations about equilibrium also simplify the mathematical analysis of the system response by allowing processes to be described by linear versions of their full constitutive equations.

Three types of transient methods are commonly used to study the dynamics of physical and chemical systems: step changes, pulses, and harmonic perturbations[1]. All of them contain the required information to measure the rates of processes taking place within the system. They can be carried out within constant volume (closed) or constant pressure (open) systems. The method of choice depends largely on the specific features of the system (e.g., gas or liquid phases, reactive or non-reactive, ...).

Step changes are simple to carry out experimentally. The dynamics of individual steps in complex systems, however, are difficult to deconvolute because they commonly appear in the system response as a sum of exponential terms that cannot be readily separated into its individual components. Only the magnitude of the step change can be varied and it is usually kept small in order to avoid highly non-linear responses. Mathematical analyses of step changes require the solution of time-dependent equations.

Pulse techniques are experimentally more demanding and often difficult to carry out with small amplitude fluctuations, but they introduce additional variables, such as the width of the pulse and the time elapsed between pulses. These features allow better access to multiple dynamic processes in complex systems. The analysis of the system response also requires the solution of transient equations. Fourier-Transform techniques are often used to analyze the system response in frequency domain because pulse techniques probe a continuun spectrum of frequencies. Pulses, however, lack the characteristic frequency (relaxation time) introduced by harmonic oscillations in frequency response (FR) experiments in which the rate of a given process can be directly probed with less interference from concurrent processes.

Harmonic perturbations of the forcing variable require even greater experimental sophistication but allow the solution of the describing equations in the frequency domain. The frequency of the oscillations introduces an additional degree of freedom that can be used to decouple individual steps occurring with different characteristic relaxation times. Thus, the added experimental complexity of these FR methods is balanced by their ability to probe directly the natural relaxation times of several concurrent dynamic processes within a complex system.

Sinusoidal perturbations have been widely used to probe the dynamics of many systems. Available studies vary widely in scope, complexity, and in their applications to many specific dynamic phenomena in gases, liquids, solids, and porous structures (Table 1). They range from analyses of chromatographic separation, dispersion, and reactions in beds of porous particles to the measurement of dynamic processes in complex biochemical systems and to the optimization of chemical reactors.

In this report, we restrict our discussion to the use of FR methods as an analytical probe of dynamic processes occurring within porous materials, commonly used as adsorbents and as heterogeneous catalysts. Specifically, we describe the use of these methods in measurements of adsorption kinetics on non-uniform surfaces and of diffusive properties within zeolitic and mesoporous solids. Their more recent use in measurements of reaction parameters and mechanisms in heterogeneous catalysis is also briefly described.

1.2 FR Methods

Angstrom[2] applied a FR technique to the analysis of heat transfer in a conducting rod. He measured the thermal conductivity of a material by imposing a sinusoidal temperature change at one end of a rod and measuring the resulting temperature fluctuation at a distance away from the source. This appears to be the first application of FR methods to the determination of kinetic parameters in dynamic systems.

In more recent pioneering work, Rosen and Winsche[8] theoretically described the use of (large amplitude) sinusoidal concentration changes to study kinetic and diffusion processes in chromatographic separation columns. They showed how periodic oscillations conveniently decouple multiple dynamic processes with different characteristic relaxation times. More importantly, they found that processes occurring in series can be described by a sum of individual dynamic resistances (impedances) containing the dynamic parameters and the diffusive and adsorptive capacities of each process. They developed impedance functions for a number of cases related to chromatographic separations: diffusion within porous solids, adsorption-desorption reactions, and diffusion coupled with external mass transfer. This work provided key insights that would develop later in applications of FR to the study of adsorption and diffusion processes within porous heterogeneous catalysts.

Eigen[55] studied fast chemical reactions in solution using several types of relaxation methods. He developed mathematical treatments for step, pulse, and frequency perturbations and obtained kinetic constants for several acid-base and hydrolysis reactions. Eigen and deMaeyer[56] later provided a comprehensive treatment of relaxation methods, which included the theoretical basis of FR methods for determining the kinetic constants of chemical reactions.

Naphtali and Polinski[60,61] first applied small amplitude FR methods to adsorption processes in porous catalytic solids. They studied the rate of adsorption of hydrogen on supported Ni. For the specific case of a Langmuir rate equation, they derived FR functions for a closed system subject to sinusoidal volume fluctuations of small amplitude. This response function was separated into components that were in-phase (real) and out-of-phase (imaginary) with the applied volume perturbation. The latter component separates the response of different types of sites on non-uniform surfaces.

Evnochides and Henley[3] also made important contributions to the development of FR by measuring the solubility and diffusivity of ethane in polyethylene films. Their work clearly showed how the capacities (solubility) and dynamics (diffusivity) can be obtained simultaneously from FR data.

After these pionering studies[3,8,55,56,60,61] Yasuda and co-workers[62-74] significantly extended the application of FR to a wide range of physical and chemical processes. Two seminal papers, one on adsorption[62] and one on diffusion[65], best illustrate the key contributions of this group. This work combined a unified theoretical approach, lacking in previous studies, with an effective design of experimental methods. New users of FR techniques almost invariably follow these experimental methods and interpretation procedures, particularly the form of the response functions proposed for adsorption and diffusion processes by this group.

Several other investigators later applied FR methods to the study of diffusion and adsorption in porous adsorbents and catalytic materials. Rees and co-workers[75-83] have extensively examined the diffusion of gases within zeolites. Marcelin and co-workers[84-87] have examined the role of supports and promoters on the kinetics of hydrogen adsorption on supported Rh catalysts. Li et al.[88,89] determined adsorption and desorption constants of CO on a Pt/SiO_2 catalyst by using frequency-modulated concentrations in a flow system combined with infrared measurements of the CO surface concentrations. Our own recent work in this area[90] has extended the applications of FR methods to diffusion and coupled diffusion-adsorption processes within mesoporous materials. These materials and processes were not previously examined because of experimental contraints and because appropriate theoretical response functions were unavailable.

The preceeding discussion provides a brief historical perspective of the most critical developments in the evolution of the FR technique. Additional details about the experiments, concepts, and applications are discussed in the sections that follow.

2. Concepts and Applications of FR

2.1 Approach

The basic principle of FR methods is that a system subject to a periodic perturbation produces a periodic response that has a lower amplitude and is shifted in phase (phase lag) with respect to the input[91-93]. The magnitude of the amplitude attenuation and the phase lag are directly related to the capacity and dynamics of the rate processes occurring within the system. The input signal in closed systems is typically a sinusoidal variation in volume; in open systems, sinusoidal changes in concentration or flow rate are common.

FR techniques have been used to study many physical and chemical phenomena in flow and batch systems (Table 1). Though the basic principles are common to all FR applications, our discussion focuses on gaseous batch systems subject to sinusoidal volume perturbations. This has been the preferred route for obtaining kinetic parameters in porous adsorbents and catalytic materials. Volume changes are attractive because of their experimental simplicity and because the rate of diffusion and surface reactions typically responds to the resulting change in gas phase concentration.

2.2 Experimental Methods

FR experiments usually involve a harmonic perturbation of the volume of a closed system using bellows or moving plate devices coupled mechanically to rotary motors. The resulting change in pressure is attenuated by the capacity of the solid to accommodate this pressure change through adsorption, diffusion, or reaction processes that decrease the number of molecules in the surrounding gas phase. The system pressure or concentration must be monitored with high accuracy and fast time resolution in order to establish the signal attenuation and the phase lag between the volume and pressure fluctuations at each forcing frequency. Pressures or concentrations are usually measured using pressure gauges with rapid response, mass spectrometry, or other concentration-sensitive analytical methods.

These measurements are especially challenging at the low and high frequency ends of the spectrum. Amplitude changes and phase lags must be acquired over several (5-10) steady-state cycles; thus, the number of data points and the time requirements are quite extensive at low frequencies (< 0.1 Hz), where accuracy is essential to establish the capacity of the dynamic process. At high frequencies (> 5 Hz), pure sine waves are difficult to generate without higher harmonics. In addition, data must be acquired rapidly in order to ensure a sufficient number of experimental data points (> 50) within each fluctuation period and accuracy becomes essential for detecting the presence of several concurrent fast processes within the dynamic system. At both high and low frequencies, phase lags become small and data acquisition and analysis methods

must be able to detect accurately phase lags of order of 0.1% of a fluctuation period and amplitude attenuations of the order of 1% of the total amplitude change.

Open systems have also been used to measure chemical reaction rates on porous solids[5,88,89]. In these systems, concentration changes are imposed to the inlet stream by synchronized mass flow controllers or by reciprocating pistons. The resulting changes at the exit stream[5], or in the adsorbed phase[88,89], are measured using mass spectrometry, surface-sensitive spectroscopies, and other analytical techniques. Mathematical and experimental descriptions of harmonic perturbations in open systems have been recently discussed by Schrieffer and Sinfelt[94].

The experimental set-up and methods of our closed FR system are typical of those reported by others[60,61,63,80]. Our apparatus consists of a closed system volume (142 cm^3, all quartz) contained within a controlled temperature box (223-423 K) and evacuated by mechanical and turbomolecular pumps to pressures as low as 10^{-9} Pa. The sample cell can be locally heated to higher temperatures (873 K) by placing it within a resistively heated furnace. The system volume is designed to minimize hydrodynamic delays and can be perturbed by small sinusoidal fluctuations (1.96 cm^3, 1.4% of system volume) around its equilibrium volume at frequencies between 0.01 and 10 Hz. All data are corrected by subtracting the response of an identical system volume containing no adsorbing or diffusing solids. This procedure removes any hydrodynamic or electronic delays unrelated to the dynamics of chemical and transport processes of interest.

Volume fluctuations are introduced using a stainless steel bellows actuated by a variable-speed rotary electric motor fitted with an eccentric cam. The position of the bellows is determined by a linear variable differential transformer that measures the forcing volume perturbation. The system pressure fluctuations are measured using a differential pressure gauge (MKS Model 223 BD, 0-130 Pa) and the resulting pressure and volume data are acquired and stored using a Dell PC-AT 320 computer and LabTech Notebook software. Turbo Pascal codes were used to control input voltages to the motor and to calculate phase lags, amplitudes, and response functions from raw pressure and volume data. Response functions are calculated after the experiments by subtracting the results of sample and blank experiments over the frequency range required to access the dynamic processes of interest.

2.3 Data Analysis

FR techniques require theoretical models to describe how the dynamic processes affect the amplitude attenuation and the phase lag at each forcing frequency. Such models vary widely in complexity, depending on the type of system and phenomena under study. The model must account for all dynamic processes involved in order to describe accurately the system response and the dynamic parameters. This includes any extraneous dynamic processes or delays caused by instrumentation (e.g., pressure transducers) or reactor hydrodynamics (connecting lines and

volumes). Such processes are preferably substracted out of the system response by controlled blank experiments instead of including their effects in the describing models.

The solution of mass conservation equations for the closed system leads to mathematical expressions, which relate the system response to the input signal as a function of frequency. Such expressions contain the system capacities and dynamic constants. These parameters are then calculated using least squares procedures that minimize the difference between theoretical and measured response functions.

The magnitude of the input perturbation is usually kept small (< 5%) in order to simplify the data analysis. This ensures that the describing equations can be used in linearized form, from which analytical response functions can be obtained. This mathematical benefit, however, requires accurate measurements of the magnitude and phase angle of small amplitude fluctuations.

Response functions have been usually described by real and imaginary components that arise naturally from mathematical treatments of the processes using complex variables. We discuss previous results using this terminology and show later that complex transfer functions (i.e., the amplitude of the pressure response divided by the amplitude of the applied volume perturbation) also contain all required information to describe the dynamic response in terms of their capacities and kinetic parameters.

2.3.1 Available Theoretical Results

In this section, we examine available theoretical results that describe the FR of dynamic processes in porous catalysts and adsorbents. Specifically, we describe how the mathematical equations and the FR data are used to obtain the dynamic constants. We review FR functions for adsorption (2.3.1.1.) and diffusion (2.3.1.2) only. These are the only processes for which sufficiently general mathematical treatments exist. The treatment of diffusion is a phenomenological description developed for zeolitic materials. Our more general description of coupled adsorption and diffusion processes within mesoporous materials is presented in Section 2.3.2.

A general theory for describing the FR of open or closed systems undergoing chemical reactions is not yet available. Specific applications to reactive systems and some early mathematical treatments are described later in Section 2.4.4. Extensive references to analyses of other applications of FR methods are given in Table 1.

2.3.1.1 Adsorption

Yasuda[62] generalized the FR study of adsorption-desorption dynamics on non-uniform surfaces. He derived the following in-phase and out-of-phase response functions based on a general adsorption-desorption rate equation $R_j(P,S_j)$:

$$\frac{v}{p}\cos\phi - 1 = \sum_j \frac{K_j / K_{-j}}{1 + (\omega / K_{-j})^2} \qquad \text{(in-phase, real)} \qquad (1)$$

$$\frac{v}{p}\sin\phi = \sum_j \frac{\omega / K_{-j}}{1 + (\omega / K_{-j})^2} \qquad \text{(out-of-phase, imaginary)}, \qquad (2)$$

where

$$K_j = \frac{RT}{V_e}\left(\frac{\partial R_j}{\partial P}\right)_e \text{ and } K_{-j} = -\left(\frac{\partial R_j}{\partial S_j}\right)_e \qquad (3)$$

The measured quantities v, p, and ϕ represent the volume amplitude, the pressure amplitude, and the phase lag between the two, respectively. Eqns. (1)-(3) apply in general for any adsorption-desorption rate equation R_j. Eqns. (1) and (2) contain two parameters K_j and K_{-j} for each class of sites j; these parameters are related to the adsorption and desorption kinetic constants by Eqn. (3).

The main features of the in-phase and out-of-phase components for adsorption of a single species are shown in Figure 1, where the abscissa is a dimensionless frequency ω/K_{-j}. At both low and high frequencies, the out-of-phase (imaginary) component approaches zero because there is no phase lag between the applied volume perturbation and the pressure response; low frequencies allow sufficient time for the system to respond without delay, while high frequencies prevent adsorption changes from occurring and the phase lag also approaches zero. The in-phase (real) component approaches zero at high frequencies because the volume perturbation is not attenuated by adsorption at the solid surfaces.

As suggested earlier by Naphtali and Polinski[60], Yasuda[62] referred to Eqn. (2) as an adsorption rate spectrum because K_{-j} is determined by the position where local maxima appeared. The out-of-phase component reaches a maximum when the forcing frequency equals K_{-j} (i.e., the characteristic relaxation time of the adsorption-desorption process) and at low frequencies, the in-phase component approaches K_j/K_{-j}. As shown by Eqn.(3) and the kinetic rate equation $R_j(P,S_j)$, K_j/K_{-j} becomes proportional to the gradient of the adsorption isotherm:

$$K = \frac{K_j}{K_{-j}} = \frac{RT}{V_e}\left(\frac{\partial S_j}{\partial P}\right)_e \tag{4}$$

This result emphasizes that FR is a differential technique that depends only on the local gradient of the adsorption isotherm near the equilibrium pressure P_e and not on the amount adsorbed. K therefore measures the capacity of the kinetic process to respond to changes in pressures. Accordingly, a saturated surface (K=0, species j) prevents the determination of its kinetic adsorption-desorption constants during FR experiments; fluctuations in the gas phase composition of that species do not change its concentration on the adsorbed phase. Another factor that prevents the detection of dynamic species is the lack of an adequate range of experimental frequencies. When these frequencies (ω) are compared to the characteristic relaxation times of the adsorption-desorption processes (K_{-j}), two main cases can be distinguished:

a) $K_{-j} < \omega$: low frequency limit-too fast to detect slow processes; no response appears on either the real or the imaginary components of the response function, and

b) $K_{-j} > \omega$: high frequency limit-too slow to detect fast relaxation processes; a flat horizontal line appears on the real response function while no corresponding peak is observed on the imaginary component.

The first case (a) provides no information about adsorption-desorption dynamics. The second case (b) gives information on the capacity (K) but not on the kinetics of adsorption. Only when $(K_{-j})_{fast} < \omega < (K_{-j})_{slow}$ can the FR experiments reveal the capacities and kinetics of every adsorption-desorption process involved.

For non-dissociative Langmuir adsorption [$dS_j/dt=R_j=k_{aj}P(N-S_j)-k_{dj}S_j$], the parameters K_j and K_{-j} become:

$$K_{-j} = k_{aj}P_e + k_{dj} \quad \text{and} \quad K_j = \frac{RT}{V_e}\left(\frac{N}{k_{aj}^{-1} + k_{dj}^{-1}P_e}\right) \tag{5}$$

The validity of the Langmuir expression can be confirmed by the correct dependence of K_{-j} and K_j on P_e and $1/P_e$, respectively. For molecules that dissociate on a non-uniform surface [$dS_j/dt=k_{aj}P(N-S_j)^2-k_{dj}S_j^2$], K_j and K_{-j} are given by[87]:

$$K_{-j} = 2N\sqrt{k_{aj}k_{dj}P_e} \quad \text{and} \quad K_j = \frac{RT}{V_e}\left(\frac{N^2}{(k_{aj}^{-1/2} + k_{dj}^{-1/2}P_e^{1/2})^2}\right) \tag{6}$$

In this case, the dissociative Langmuir rate equation requires that both K_{-j} and $/\sqrt{K_j}$ be proportional to $\sqrt{P_e}$. Expressions for K_j and K_{-j} can be readily derived for other adsorption rate equations by simply using the definitions given in Eqn.(3). Examples of the use of Eqns. (5)-(6) in adsorption-desorption processes are discussed in Section 2.4.1.

2.3.1.2 Diffusion

Here, we briefly review the equations required to describe the system FR for diffusion processes occurring within porous slabs or spheres. The material balance and boundary condition at the particle surface:

$$\frac{\partial C}{\partial t} = D\nabla^2 C, \quad C(r_o, t) = KP(t), \tag{7}$$

leads to the following in-phase and out-of-phase components of the pressure response[65]:

$$\frac{v}{p}\cos\phi - 1 = K\frac{1}{\eta}\left(\frac{\sinh\eta + \sin\eta}{\cosh\eta + \cos\eta}\right) \qquad \text{(slabs)} \tag{8}$$

$$= K\frac{3}{\eta}\left(\frac{\sinh\eta - \sin\eta}{\cosh\eta - \cos\eta}\right) \qquad \text{(spheres)} \tag{9}$$

$$\frac{v}{p}\sin\phi \quad = K\frac{1}{\eta}\left(\frac{\sinh\eta - \sin\eta}{\cosh\eta + \cos\eta}\right) \qquad \text{(slabs)} \tag{10}$$

$$= K\frac{6}{\eta}\left[\frac{1}{2}\left(\frac{\sinh\eta + \sin\eta}{\cosh\eta - \cos\eta}\right) - \frac{1}{\eta}\right] \qquad \text{(spheres)} \tag{11}$$

K is again proportional to the gradient of the adsorption isotherm and it is explicitly given by Eqn. (4). The dimensionless frequency η is defined as

$$\eta = \left(2\omega r_o^2 / D\right)^{1/2}, \tag{12}$$

where r_o is the sphere radius or half the thickness of the slab.

These response functions contain an effective Fickian diffusivity (D) and a capacity term (K) as the only parameters required from experimental measurements of v, p, and ϕ. Figure 2 illustrates the in-phase and out-of-phase components for diffusion processes within porous spheres; its qualitative features also apply to slab and cylindrical particles. This figure shows that the in-phase component approaches the value of K asymptotically as ω decreases. This low

frequency limit reflects the capacity of the porous particle to "store" molecules within its pore volume as the pressure varies during one sinusoidal fluctuation (i.e., the gas fully penetrates the particles during one cycle). In contrast, both components approach zero asymptotically at high frequencies. This high frequency limit occurs when the diffusion relaxation time is greater than the characteristic period of the fluctuation and molecules cannot penetrate the porous particles during one cycle.

The conservation equation (7), used to derive the FR functions (Eqns. (8)-(11)), contains only an average concentration (C) and effective diffusion coefficient (D), which do not explicitly distinguish between intrapellet gas and adsorbed phases. This appears to be the only description available from our limited knowledge about the nature of the phase contained within small-pore materials such as zeolites. It does not generally apply to mesoporous structures (mean pore radius > 20Å), within which adsorption and diffusion occurs concurrently in distinguishable gas and surface phases. As we show in the following section, this distinction allow us to account explicitly for the rate of interchange between gas and surface phases and for their respective diffusivities in these two phases.

2.3.2 New Mathematical Treatments

In the previous section, we described FR functions for independent adsorption and diffusion processes. Such equations do not account for the coupling of reaction and transport processes occurring in series. Here, we show how mathematical perturbation techniques offer an efficient method to derive general transfer functions when several dynamic processes occur simultaneously. We illustrate this approach by obtaining analytical transfer functions for coupled adsorption, gas-phase diffusion, and surface diffusion of multicomponent mixtures within mesoporous solids. These generalized transfer functions contain the results described in Section 2.3.1.1 and 2.3.1.2 as special cases for uncoupled adsorption and diffusion processes.

Our objective here is to outline a procedure for obtaining general FR transfer functions for mesoporous materials in analytical form. In this derivation, we make some simplifying assumptions. Extending the analysis to non-equimolar reacting systems is straightforward but not considered here because of the lack of generality introduced by the selection of case-specific reaction mechanisms.

We consider a closed system of volume V_e containing M species initially in equilibrium with a mesoporous material of total pore volume V_p and density ρ_p. V_e is the total volume of the system, excluding the volume occupied by the particles. The system volume is varied sinusoidally with a small amplitude at each frequency ω. The particles are assumed to be of uniform size, r_0, where r_0 is half the thickness of a slab or the radius of a cylindrical or spherical pellet. The internal solid surface is assumed to be energetically non-uniform, allowing species to adsorb with

different binding energies and kinetics onto L distinct types of sites. The adsorption on each type of site can be either molecular (α=1) or dissociative (α=2).

We also assume that mean free paths for each species are greater than the mean pore radius of the mesoporous particles. This corresponds to Knudsen diffusion within particles, for which individual diffusivities depend on pore size, temperature, and molecular weight but not on the presence or the identity of other molecules. This assumption is accurate for most molecules within high surface area adsorbents and support materials at usual catalytic conditions of pressure and temperature.

The conservation equations and boundary conditions for gaseous species (n=1,...,M) within mesoporous particles are:

$$\frac{\partial C_n}{\partial t} = D_n \nabla^2 C_n - \rho_p \sum_{\ell=1}^{L} [k_{an\ell} C_n (N - \sum_{j=1}^{M} S_j)^{\alpha} - k_{dn\ell} S_n^{\alpha}] \tag{13}$$

$$C_n(r_o,t) = \frac{P_n(t)}{RT}; \quad \frac{\partial C_n}{\partial r}(0,t) = 0; \quad C_n(r,0) = C_{ne} \quad , \tag{14}$$

where C_n and D_n are the molar concentration and effective diffusivity of species n within pore voids, and $k_{an\ell}$ and $k_{dn\ell}$ are the adsorption and desorption constants of species n on sites of type ℓ. $P_n(t)$ is the partial pressure of species n within the extrapellet system volume.

The corresponding material balances and boundary conditions at pore surfaces within the mesoporous structure are:

$$\frac{\partial S_n}{\partial t} = d_n \nabla^2 S_n + \sum_{\ell=1}^{L} [k_{an\ell} C_n (N - \sum_{j=1}^{M} S_j)^{\alpha} - k_{dn\ell} S_n^{\alpha}] \tag{15}$$

$$S_n(r_o,t) = \frac{N[K_{n\ell} C_n(r_o,t)]^{1/\alpha}}{1 + \sum_{j=1}^{M} [K_{j\ell} C_j(r_o,t)]^{1/\alpha}}; \quad \frac{\partial S_n}{\partial r}(0,t) = 0; \quad S_n(r,0) = S_{ne} \quad , \tag{16}$$

where S_n and d_n are the molar concentration and effective diffusivity of species n on pore surfaces, and $K_{n\ell}$ is the ratio of adsorption and desorption constants of species n on sites of type ℓ. N is the saturation coverage at the conditions of the experiment.

For a closed system, mass conservation of each species n requires that:

$$\frac{d}{dt}\left(\frac{P_n V}{RT} + \int_o^{r_o} s\left(\frac{r}{r_o}\right)^{s-1} [V_p C_n + S_n] d\left(\frac{r}{r_o}\right) \right) = 0 \quad ; \tag{17}$$

s is a geometric factor that equals 1, 2, or 3 for slabs, cylinders, or spherical particles, respectively. As discussed earlier, we have separated the amounts adsorbed on the surface (S_n) from those contained within intraparticle gas phase voids (V_pC_n). Our approach also separates dynamic processes occurring within each phase and their respective capacities.

Equations (13)-(17) completely describe the dynamic behavior of a closed system perturbed from equilibrium by a change in the system volume. As shown in the Appendix, the pressure response of this system is described by the following analytical transfer function:

$$H(i\omega) = \sum_{n=1}^{M} \left(\frac{\gamma_n}{1 + \frac{V_p}{V_e} E_n + \frac{V_n}{V_e} F_n} \right) \tag{18}$$

$H(i\omega)$ contains a real and an imaginary component and describes the simultaneous (gas and surface) diffusion and adsorption of M species onto L distinct types of sites. In analogy with the FR response functions of Sections 2.3.1.1 and 2.3.1.2, the following relationships apply:

$$p / v = \|H(i\omega)\| = \sqrt{[Re(H)]^2 + [Im(H)]^2} \tag{19}$$

$$\phi = \tan^{-1}[Im(H) / Re(H)] \tag{20}$$

Eqn. (18) conveniently describes the system FR and contains the same information as the real and imaginary components used in previous studies. Its derivation uses mathematical perturbation techniques that are easily extended to multiple simultaneous processes. The form of the transfer function also provides useful physical insight into how coupling between dynamic processes is reflected in the response curves. For example, the magnitude of the transfer function H (Eqn. 19) is always less than or equal to one and is a direct measure of the amplitude attenuation undergone by the input signal, i.e., it measures the amplitude ratio between the pressure response and the volume perturbation. The phase lag between the applied and the output signal is simply given by Eqn. (20). Also, the value of the denominator at low frequencies gives the sum of the capacities of all dynamic processes accessible in the experimental frequency range. Thus, V_p/V_e is the capacity associated with the diffusion process, which is a pore volume shared by all diffusing species, while V_n/V_e is the capacity associated with the adsorption process of each species n on the pore surfaces; E_n and F_n are their corresponding dynamic terms, which measure the rate at which the void and surface reservoirs share molecules with the extrapellet gas phase at each forcing frequency. These features reinforce the usefulness of the classical Bode

diagrams ($\|H(i\omega)\|$ vs. ω and ϕ vs. ω), customarily used in the analysis of FR data in many engineering applications[91-93]. Figures 3 and 4 show the equivalent Bode diagrams for the adsorption and diffusion examples presented in Figures 1 and 2, respectively. These figures provide a direct representation of the amplitude attenuation and phase lag as a function of the applied frequency.

The analytical transfer function $H(i\omega)$ contains all the special cases derived previously (Sections 2.3.1.1 and 2.3.1.2) for independent diffusion and adsorption (dissociative and molecular) processes within particles of slab, cylindrical or spherical geometry. Such limiting cases can be obtained by appropriately selecting the parameters M, L, s, d_n, and α that appear in Eqn.(18) and related formulae in the Appendix. For example, the transfer function for coupled gas diffusion (d_n=0) and non-dissociative adsorption (α=1) of a single species (M=1) on homogeneous sites (L=1) within spherical particles (s=3) becomes:

$$H(i\omega) = \frac{1}{1 + \frac{V_p}{V_e} E_1 + \frac{V_1}{V_c} F_1} \quad , \tag{21}$$

where

$$E_1 = 3(\coth\psi_1 - 1/\psi_1)/\psi_1; \quad F_1 = \lambda E_1 \tag{22}$$

$$\lambda = k_{d11}/[k_{d11}/(1 - S_{1e}/N) + i\omega]; \quad \psi_1^2 = (i\omega r_o^2/D_1)[1 + \rho_p S_{1e}\lambda/C_{1e}] \tag{23}$$

For pure diffusion (S_{1e}=0), Eqns. (21)-(23) confirm that the real and imaginary components of H (expressed as $(v/p)\cos\phi - 1$ and $(v/p)\sin\phi$, respectively) approach each other and tend asymptotically to zero at high frequencies. The imaginary component also approaches zero at low frequencies, whereas the real component approaches V_p/V_e. This latter limit, which can also be written as $(RT/V_e)dn_v/dP_1$ (n_v: total number moles contained within the pore voids), is directly related to the capacity of the porous solid to accommodate a fluctuation in pressure. Clearly, for non-adsorbing mesoporous solids, the capacity is given by the intraparticle pore volume divided by the total volume of the system. The real and imaginary components for diffusion given by Eqn. (21) are identical to those previously shown as Eqns. (9) and (11).

For pure adsorption-desorption processes (V_p=0 and D_1=∞), the real and imaginary components of the response function H are also identical to those derived in Section 2.3.1.2 (Eqns. (1) and (2)). Our derivation shows how independent adsorption and diffusion processes can be recovered from an overall transfer function and, more importantly, how this transfer function rigorously accounts for the coupling between these processes when they occur at comparable time scales. Obviously, when diffusion is very fast compared to adsorption, coupling

between the two processes does not occur and the transfer function naturally segregates the adsorption-desorption process at the lower frequencies and the diffusion process at the higher frequencies. Thus, during the period of one fluctuation, rapid diffusion quickly establishes thermodynamic equilibrium between the extraparticle system volume and the intraparticle gas phase. This situation separates the dynamics of the adsorption process from transport effects and allows measurements of pure adsorption kinetics. It is often achieved in practice by decreasing the size of the porous particles.

When adsorption-desorption processes are much faster or occur in a time scale comparable to diffusion processes (as is common in many applications), the coupling is unavoidable. Therefore, the intraparticle transport rate is insufficient to establish thermodynamic equilibrium with the external particle surface within one perturbation period (except at very low frequencies) and the molecules adsorb as soon as they penetrate the particles. The net effect of simultaneous or fast adsorption is to impose a greater load to the diffusion process (Eqn. 23; last term in square brackets). The use of transfer functions for diffusion, which ignore fast adsorption-desorption processes is incorrect. Similarly, the mere addition of adsorption and diffusion transfer functions to describe the overall process dynamics is also incorrect.

2.4 Applications

In Sections 2.3.1.1 and 2.3.1.2, we introduced the basic features of the FR of adsorption and diffusion processes in batch systems subject to small volume perturbations. Here, we summarize some key experimental studies, verify the theoretical concepts, and illustrate the historical development of these techniques. We select examples of their use in measurements of adsorption and diffusion rates within zeolites and mesoporous solids. Also, we critically evaluate the advantages and complexities of the FR technique in the study of dynamic phenomena in gas-solid systems.

We continue to make a distinction between the concepts and results applicable to zeolites and to mesoporous structures, consistent with our discussion in Section 2.3.2. This distinction is required in order to account for intrinsic differences in the mechanistic details involved in diffusion and adsorption within small and large pore materials.

2.4.1 Adsorption

Naphtali and Polinski [60,61] first used a FR technique to study the dynamics of adsorption-desorption processes on heterogenous catalysts. They established theoretically that the imaginary component of the response function isolates the contributions from distinct adsorption-desorption processes with different relaxation times (i.e., a linear superposition principle). They described this function as an "adsorption rate spectrum" because distinct, although broad, maxima appear at

certain characteristic frequencies. The location of the maxima reflect the relaxation times of one or more species in dynamic equilibrium with the surface.

They verified experimentally that several forms of adsorbed hydrogen could be detected on Ni surfaces by varying the frequency of the volume modulation. Two maxima appear in the imaginary component of the response function (Figure 5), suggesting that the system response consists of at least two kinetic processes occurring in parallel but with different characteristic relaxation times. A curve-fitting analysis using Langmuir rate equations suggested that four species were required in order to describe the measured adsorption rate spectrum. The characteristic relaxation times of those four species are shown by the arrows in Figure 5.

Naphtali and Polinski[60,61] showed that the FR of a closed system was suitable for the study of kinetics of adsorption and desorption on non-uniform surfaces. The results of Figure 5, however, also reveal a difficulty with the technique: a deconvolution process is still required to determine accurately the number of distinct species or sites contributing to the measured adsorption rate spectrum. In this case, four species led to only two broad peaks in the spectrum. Unfortunately, it is a feature of FR that each contributing species does not appear as a narrow individual peak in the rate spectrum (see Figure 1), but as a peak extending over a broad frequency range and possibly overlapping with other adsorption or diffusion processes. In general, the response function is a complex "fingerprint", whose mathematical deconvolution into individual species may not be unique. This becomes a serious limitation when relaxation times for several species or processes are similar and the resulting features cannot be uniquely isolated using curve fitting or deconvolution procedures.

Yasuda[62,63] provided strong evidence for the reliability and accuracy of FR methods in studies of adsorption processes, clarified several important aspects related to experimental procedures and requirements, and developed a rigorous mathematical framework to obtain the kinetic parameters for arbitrary adsorption kinetics from FR data. These contributions were critical to the evolution of FR techniques to their present state.

Figures 6-8 illustrate Yasuda's key contributions to the study of adsorption kinetics using FR techniques[63]. Figures 6 and 7 show the real and imaginary response functions for ethylene adsorption on ZnO at 253 K. He used Eqns. (1) and (2) and least squares fitting procedures to determine that three kinetically distinct species (I, II, and III) were required to describe the response data (dashed lines in Figures 6 and 7). He concluded from his analysis of the response functions that species I was involved in an adsorption-desorption process with a very short relaxation time, which could not be accessed in his experimental frequency range; therefore, a corresponding peak did not appear in the imaginary response function (Figure 7). He described species I as physisorbed ethylene. By varying the ethylene pressure, he showed that species II and III corresponded to chemisorbed ethylene obeying a Langmuir adsorption equation (i.e., the

parameters K_j and K_{-j} followed the pressure dependence suggested by Eqn. (5)). Yasuda's[63] findings were in good agreement with independent steady-state chemisorption measurements by Dent and Kokes[95].

Yasuda[63] noted that species I-III, whose amount is proportional to the height of the real response function in the limit of zero frequency in Figure 6, could not account for all the ethylene adsorbed on ZnO and measured independently from adsorption isotherms at 253 K (Figure 8). He proposed that a species IV (dashed circles), which remained after desorption of species I-III, desorbed very slowly and its relaxation time was much longer than those accessible in his FR apparatus. He suggested that such species also exhibited a Langmuir behavior and could be dynamically detected by carrying out experiments at much lower frequencies and ethylene pressures.

The experiments described in Figures 6-8 also illustrate other important features of FR techniques[63]. First, fast adsorption-desorption processes may not be accessible even at the highest experimental frequencies and do not appear in the adsorption rate spectrum (imaginary response); they are, however, detected as a contributing capacity in the real response function. In such cases, only the capacity but not the kinetics of the process can be determined from FR measurements. Also, comparisons of the value of the real response function at very low frequency with capacities calculated from adsorption isotherms provides a measure of what fraction of the absorbing sites are detected in the FR experiment. FR measurements cannot account for all available sites when experimental frequencies do not span the longest relaxation times of adsorbed species, because such species become permanently "trapped" at the solid surfaces during the period of one fluctuation. Another rather common situation can prevent the detection of adsorbed species, even when the frequency range spans the adsorption relaxation times; it occurs when sites are saturated with adsorbed species (K=0) at the conditions of the experiment, because the FR method is sensitive to the gradient of the adsorption isotherm and not the amount adsorbed.

Marcelin and co-workers[84-87] and Gonzalez and co-workers[88,89] contributed several important advances and illustrative examples in FR measurements of adsorption dynamics. Marcelin et al.[87] examined the role of support and promoters on the kinetics of hydrogen adsorption on supported Rh catalysts (Figure 9). They observed several kinetically distinct sites, on which adsorption dynamics varied with changes in support, promoter, and adsorption temperature. At low temperatures (321 K, not shown), the pressure dependence of the kinetic parameters K_j and K_{-j} suggested non-dissociative Langmuir kinetics. At high temperature (433 K, Figure 9), however, the pressure dependence of adsorption rates showed that the adsorption occurred with dissociative Langmuir kinetics (Eqn.(6)).

Li et al.[89] determined adsorption and desorption rate constants of CO on Pt/SiO_2 by modulating the gas phase concentration in a flow system and measuring the resulting fluctuations in CO surface concentration using infrared spectroscopy. In their treatment, kinetic parameters could be determined from a discontinuity of the phase lag response at a critical frequency, i.e., a resonant frequency at which the residence time in the reactor becomes equal to the relaxation time of the adsorption-desorption process. Figure 10 shows this discontinuity of the phase lag at two different temperatures. An attractive feature of their approach is the direct monitoring of the concentration of adsorbed species during frequency modulation of gas phase concentrations.

2.4.2 Diffusion

2.4.2.1 Zeolites

Evnochides and Henley[3] first applied FR techniques to diffusion by measuring the diffusivity of ethane within low density polyethylene films using a closed system subject to small sinusoidal changes in pressure. They related the amplitude ratio and phase lag to the diffusivity and solubility of a gas within the permeable polymer. Figures 11 and 12 show the excellent agreement they obtained between theoretical predictions (solid lines) and experimental results (open squares and circles). Their estimates of effective diffusivities were in close agreement with those obtained using other transient techniques.

In their study, a very narrow frequency range (less than one decade) was sufficient to produce measurable changes in both amplitude attenuation and phase lag. Experimentally, this is very convenient because it requires data acquisition at only a few discrete frequencies. Also, the excellent agreement between theory and experiment suggests that other kinetic processes did not interfere with diffusion in their experimental frequency range. As a result, they concluded that measurements at a single frequency were sufficient to determine the solubility and diffusivity of ethane in the polymer film. Overall, Figures 11 and 12 illustrate classical results of the FR method (Bode diagram) relating the attenuation of the input signal and the phase lag of the response to the forcing frequency.

Yasuda[65] extended the use of the FR methods to determine diffusivities of gases within zeolitic solids. In his treatment, he preserved the mathematical framework developed previously for adsorption-desorption processes[62]. The response functions were again expressed in terms of real and imaginary components, but now contained the diffusion capacity and the diffusivity as the parameters required from experimental data. This theoretical framework provided the basis for his many later studies of diffusion of various molecules and their mixtures within zeolitic solids[67-71,73,74]. Rees and co-workers[75-83] have extensively applied the formalism of Yasuda to diffusivity measurements in zeolites and also extended the experimentally accessible frequency range. In what follows, we highlight some key examples that illustrate the validity of the

theoretical analyses and also some complications that must be rigorously treated in order to describe accurately the experimental system response.

As discussed in Section 2.3.1.2, FR measurements of diffusion within zeolitic solids have been described using models that do not distinguish between diffusing and adsorbed phases within zeolite channels. These models treat the dynamic process as diffusion into a pore space with a reservoir capacity equivalent to the sum of the geometrical channel void and any adsorption volumes and equal to the total uptake during adsorption isotherms. This assumption is unlikely to hold when loosely bound and strongly bound forms of the molecule co-exist within channels and interconvert slowly compared with the diffusive process. As we discuss below, many of the unusual features detected in the applications of FR to zeolitic systems may reflect the use of these incomplete models for the description of the intrinsically coupled adsorption and transport processes.

In the first application of FR methods to diffusion within zeolites, Yasuda[65] examined the diffusion of Kr in Na-mordenite at 253 K. These measurements demonstrated that FR techniques detect the dynamics of intracrystalline diffusion processes (Figure 13). Experimental data (circles and square symbols) and the best theoretical fit (solid curve) are in excellent agreement, but the real and imaginary response functions do not meet at high frequencies, even though this is predicted by theoretical treatments of pure diffusion (Figure 2). Yasuda suggested that this disagreement between data and model reflects the presence of a fast intercrystal diffusion process with relaxation times much shorter than those accessible even at the highest frequencies of the experiments. The capacity of this intercrystal reservoir (expressed as a fraction of the total system volume) is given by the magnitude of the dashed horizontal line in Figure 13.

This proposal is not unreasonable given the samples used, which consisted of compressed pellets (approx. 1 mm diameter) of micron-size zeolite crystals and containing intercrystal mesoporous voids with effective diffusivities much larger than those within zeolite channels. Equally reasonable and able to describe the form of the curves in Figure 13 is the proposal that adsorption occurs within zeolite channels with rates comparable to those of diffusion, thus introducing an additional delay and a distinct reservoir into the models used to analyze the experimental results. (See analysis of coupled adsorption and diffusion within mesoporous structures in Section 2.3.2.) This ability of more than one physical mechanism to describe with equal likelihood available experimental results underscores the critical need for rigorous accounting of all relevant dynamic processes accessible in FR measurements.

Another example of subtle features that can easily lead to erroneous diffusivity values is the effect of zeolite crystal size on the shape of the response curves. Figure 14 shows diffusivity response data for Kr diffusion in zeolite A at 195 K and the best simultaneous fit of the real and imaginary response functions assuming the crystals to be of uniform size (dotted line)[67]. The

discrepancies between the data and the model suggest that, besides diffusion, other processes may occur simultaneously during the FR experiment. It would indeed be tempting to propose that Kr may diffuse differently along various crystal directions or that various forms of intracrystalline Kr exist and diffuse differently from each other. Each of these assumptions introduce additional parameters that would improve our ability to fit the FR results, but which detract from the appropriateness of the models if the proposed representation is unrelated to the true cause of the observed effects.

Yasuda[67] opted for the simplest physical explanation of the observed discrepancies: that a distribution of zeolite crystal size, observed experimentally, broadens the response curves compared with the theoretical predictions. Indeed, when this correction was introduced into the response functions, he obtained much better agreement with the data (Figure 14, solid line) without introducing additional adjustable parameters or physical processes, but only an experimentally derived crystal size distribution.

In another study, Yasuda, et al.[73] found that FR methods gave diffusivities for light paraffins within zeolite A very different from those obtained from pulsed-field gradient NMR and adsorption rate measurements (Figure 15). Diffusivities for methane, ethane and propane measured by FR methods were about 10 times larger that those obtained from adsorption uptake rates and about 10^3-10^4 times smaller than those from nuclear magnetic resonance (NMR) methods. These authors did not give any explanations for these puzzling results. Clearly, the three methods probe the ability of molecules to move, but within different length scales. NMR measures local mobility within the distance that molecules probe during the time of an NMR pulse (10 nm); FR methods probe mobility over distances traveled during the period of one fluctuation (100 nm-1000 nm). Adsorption rates, in turn, require mobility over the entire crystal size (1-10 microns). Thus, the presence of irregular channel structures and pockets and of zeolite structural defects tends to decrease the effective diffusivities as molecules probe larger distances and sample more of these features.

Similar differences among diffusivity values obtained by these various techniques were also reported by Bülow et al.[76] for ethane and propane within large (unpelletized) crystals of ZSM5. They suggested that diffusivities measured in their FR methods were influenced by the depth of packed-beds of zeolite crystals because of intercrystal diffusion processes with relaxation times proportional to bed height. Later studies by the same group[77,80] showed how the diffusion coefficient of ethane in silicalite (a pure Si form of ZSM5) varied with bed height (Figure 16). A four-fold decrease in bed height (2.4 to 0.6 g of silicalite) increased the apparent diffusivity by a factor of about 5, consistent with an intercrystal transport resistance proportional to bed height. When small amounts of silicalite were dispersed in glass wool, diffusivities increased by an additional factor of 10^2 and approached values similar to those obtained from NMR methods.

This study[77,80] concluded that NMR and FR methods give similar diffusivity values provided that very shallow beds are used in the latter measurements. Yet, the earlier work of Yasuda[73], where bed height effects are less severe because large compressed pellets of zeolite crystals were used, still detected significant differences among the three diffusivity methods.

Later studies revealed other unusual features that could not be accounted by the simple diffusion model of Section 2.3.1.2. For example, Yasuda and Yamamoto[68] found that several dynamic processes contribute to diffusion of propane within zeolite A at 253 K (Figure 17). They concluded that experimental response curves reflected contributions from two additive (independent) diffusive processes, associated with tightly and loosely bound species within zeolite channels. Indeed, two independent diffusion processes with diffusivities differing by a factor of 10^4 describe the experimental results well (solid line in Figure 17).

Their model requires that the two types of intracrystalline propane do not interconvert or interact with each other. It is very surprising that intracrystalline propane diffusion can occur via two independent processes, considering the regularly intersecting channel structure of zeolite A. It is much more likely, and equally adept at reproducing experimental results, to consider that only one diffusion mechanism exists (that of loosely-held intracrystalline propane) and that a slow adsorption process interconverts loosely and strongly adsorbed species. This proposal now rigorously couples diffusion and adsorption steps, which cannot be described by previous diffusion models[68], but require instead treatments such as those developed in Section 2.3.2. The lumping of adsorption and diffusion in previous FR studies of zeolite diffusion restricts our ability to account for their coupling as molecules move within intracrystalline zeolite channels.

Shen and Rees[81] reported similar unusual features for n-butane and 2-butyne within silicalite. For 2-butyne, they proposed two additive and independent diffusion processes in order to describe their experimental response functions (Figure 18) and suggested that they are associated with diffusion within straight and sinusoidal channels in silicalite. Their data suggest that diffusion within straight channels is about ten times faster than within sinusoidal ones. More recently, the same authors[83] proposed a similar dual diffusion mechanism to describe the diffusion of p-xylene in silicalite at 395 K and 0.43 Torr. Yet, they found[82,83] that only straight channel diffusion was required to describe the FR curves for benzene within the same samples, a surprising result in view of the molecular and diffusive resemblance between benzene and p-xylene. These FR data may also reflect a slow adsorption process that becomes more important for p-xylene than for benzene within silicalite channels.

The additive nature of the response functions used by Shen and Rees[81,83] to interpret their FR data requires that diffusion within straight and sinusoidal channels occur independently and without kinetic communication between the two channel structures. Clearly, the two types of channels in silicalite are likely to have different capacities and diffusion dynamics. Yet, silicalite

structures consist of two types of channels that intersect once in every unit cell, suggesting that penetration by a diffusing molecule can occur by using the more efficient channel to fill the other. Thus, diffusion occurs by sequential processes in which straight channels are able to conduct molecules even at high frequencies to within a unit cell distance of every point in each sinusoidal channel. Then, the process cannot be described by two independent diffusion mechanisms and the mathematical treatment used by these authors is at best incomplete. These arguments would suggest that straight channels act as feeder pores for the sinusoidal ones and that the diffusion dynamics are exclusively associated with mobility within the larger channels. Just as likely is that diffusion occurs within both channel structures with relaxation times that are similar within the frequency resolution of their response measurements, and that the additional process is one of slow adsorption, which decreases the rate at which the diffusing species and the adsorbed phase interconvert.

Diffusion of binary mixtures within zeolites have also been studied using FR methods[68-71,83]. Figure 19 shows the example of CH_4-Kr mixtures within zeolite A at 195 K[68]. The real and imaginary components suggest the presence of more than one dynamic process at the conditions of these measurements. The authors used an extension of Fick's law to binary mixtures to derive response functions that included self (D_{11} and D_{22}) and cross-term (D_{12} and D_{21}) diffusion coefficients and which described the experimental results well. They concluded that the self-diffusivities of CH_4 and Kr (D_{11} and D_{22}) were different from those of the pure components and that their values varied significantly with mole fraction; a clear indication of molecular interactions. Similar trends were observed for the system N_2-O_2 on zeolite A at 273 K[71].

When molecules interact, response functions no longer consist of the sum of the individual contributions from each component in the mixture. An example of interacting mixtures -- p-xylene/benzene -- in silicalite, was examined by Shen and Rees[83]. Their results suggest that p-xylene diffusivities decreased markedly with increasing benzene pressures, illustrating the importance of intermolecular interaction even at very low pressures within the cramped confines of zeolite channels. Unfortunately, these conclusions were reached by analyses of response functions that apply only for non-interacting mixtures, where components are assumed to diffuse independently of each other.

2.4.2.2 Mesoporous Materials

In contrast with zeolites, diffusion and adsorption processes within mesoporous solids can be separated kinetically and geometrically. This leads to rigorous models that separate the diffusion gas phase, residing within intrapellet voids, and the adsorbed phase, located on the pore walls.

In this section, we describe our FR studies of diffusion within mesoporous silicas (Shell, S980B, 204 m^2/g, 1.16 cm^3/g, 7.0 nm average pore diameter from N_2 physisorption, 3.0 mm average sphere diameter from optical microscopy). We illustrate the ability of this technique and of our general theoretical treatment (Section 2.3.2) to detect diffusion and adsorption processes that occur independently or simultaneously within these structures. In contrast with the analysis of diffusion in zeolites presented earlier, we use here the generalized transfer function (Eqn.18), which rigorously distinguishes between intrapellet gas and adsorbed phases. First, we examine diffusion of non-adsorbing molecules (N_2 and Xe) and their mixtures in order to show how diffusivities and capacities are derived from FR measurements in mesoporous solids. Then, we present results for diffusion coupled with fast adsorption to show the importance of correctly accounting for dynamic processes occurring in series.

Figure 20 shows the diffusion FR of N_2 within silica spheres at conditions where N_2 physisorption uptakes are small (308 K, 16 Torr). Phase lags (and the imaginary component) approach zero at both low and high frequencies. At low frequencies, the observed change in amplitude reflects the gas volume required to fill entirely the intrapellet voids and the real response component approaches its asymptotic value V_p/V_e. As required by the theory, both the real and imaginary components of the response approach zero asymptotically and concurrently at high frequencies. At intermediate frequencies, phase lags and amplitude changes contain information on the dynamics of gas penetration, a process governed by Knudsen diffusion at the conditions of our experiments.

The data in Figure 20 contains the required information to determine simultaneously both the diffusivity (D) and the capacity (K) of the solid to accomodate external pressure fluctuations. According to the analysis in Section 2.3.2, K equals the ratio V_p/V_e for non-adsorbing gases within mesoporous materials. Thus, if the silica pore volume can be measured independently (e.g., by He pycnometry or Hg intrusion), one can choose to fit D only while providing the value of V_p/V_e. The solid lines in Figure 20 show the best fit using a non-linear least squares procedure to obtain K and D simultaneously. The estimated value of K coincides with the expected value V_p/V_e, showing that no other kinetic processes are accessible in the frequency range of the experiments. These results also corroborate the ability of the technique to accurately measure the intraparticle pore volume (reservoir capacity) of the silica spheres from the low frequency limit of the experiments. The agreement between the data and the theoretical reponse functions with a diffusivity value of 4.8 10^{-3} cm^2/s is excellent.

This measured N_2 diffusivity also agrees closely with values estimated from detailed transport simulations within coalesced aggregates of microspheres, which accurately describe this type of mesoporous sol-gel structures[96]. In such simulations of non-adsorbing molecules, effective diffusivities are entirely determined by the velocity of the diffusant, by the size of the

microspheres, and by the solid porosity. The prediction of these simulations, for the sample and conditions used to obtain the FR data in Figure 20, is 5.6 10^{-3} cm^2/s, a value very similar to that required to describe these data (4.8 10^{-3} cm^2/s). Effective Knudsen diffusivity measurements for non-adsorbing gases at other conditions also agree well with values predicted from these models and with their expected dependence on temperature ($D \sim T^{0.5}$), pressure ($D \sim P^0$), and diffusant molecular weight ($D \sim M_W^{-0.5}$)[90].

We have also carried out FR measurements of mixtures of non-adsorbing and non-interacting gases (N_2-Xe) within silica spheres at 398 K. In the Knudsen diffusion regime prevailing at the conditions of our experiments, molecules collide predominantly with the pore walls and diffusivities become independent of the concentration and identity of the components in the mixture. Therefore, this is a case where individual diffusion response functions can be rigorously added.

FR diffusion data for Xe-N_2 (50:50, 16 Torr) mixture within silica spheres are shown in Figures 21 and 22. The solid lines are the predicted responses using effective diffusivities for Xe and N_2, independently obtained from FR measurements using pure components, and the response functions from Section 2.3.2. Figures 21 and 22 also show the individual response functions (dashed lines) predicted for pure N_2 and pure Xe. As expected, the low frequency limit of the real response function for the mixture reaches the same asymptotic value as the corresponding response function for pure N_2 (Figure 20) because this limit measures an intrinsic property of the mesoporous material (its pore volume capacity), which is independent of the diffusion dynamics. These results demonstrate that FR methods detect Knudsen diffusivities of individual components in gaseous mixtures, but their respective diffusivities must differ by at least a factor of two.

2.4.3 Coupled Adsorption-Diffusion Within Mesoporous Structures

Isobutane isotherms at 308 K show that isobutane physisorbs on silica at the conditions of our diffusivity measurements[90]. Thus, diffusion processes must not only satisfy the filling (and emptying) of pore volume during a pressure fluctuation but also a change in the amount adsorbed. Thus, the capacity of the system, obtained from the low frequency limit of the real component of the response function, includes contributions from both physisorption and pore volume filling requirements. This capacity term appears explicitly in the denominator of Eqn.(21).

FR data for isobutane on silica at 308 K are shown in Figure 23. The real response at low frequencies is larger than for N_2 or N_2-Xe mixtures because of the larger effective capacity of this system for "storing" changes in the external gas phase concentration during a cycle. The solid lines of Figure 23 were obtained using the transfer function (Eqn. (21)) for a process coupling rapid isobutane adsorption (i.e., equilibrated adsorption) with gaseous diffusion. The agreement between the theoretical and the experimental results is again excellent. The additional capacity

due to the adsorbed phase was also independently measured from the slope of the adsorption isotherm at the same temperature of the FR experiments. The resulting effective diffusivity of isobutane in these mesoporous silica solids ($3.3\ 10^{-3}$ cm^2/s) is very similar to that predicted from Monte Carlo transport simulations[96] within such structures ($3.9\ 10^{-3}$ cm^2/s). More importantly, its magnitude properly scales with the difference in molecular weight between isobutane and N_2. Thus, FR methods and the analytical response functions of Section 2.3.2 can be used to accurately measure diffusivities in temperature and pressure regimes where significant simultaneous adsorption of diffusing molecules occurs.

2.4.4 Chemical Reactions

The kinetic behavior of chemically reacting systems has also been examined using FR techniques in both closed[35] and open[72,94] sytems. The applications are less extensive than in adsorption and diffusion processes, but they illustrate the key requirements of the technique to address kinetic and mechanistic issues in chemical reactions.

Fahidy and Perlmutter[35] studied the oxidation of SO_2 on a catalytic Pt wire contained within a well-mixed closed system by imposing a small sinusoidal fluctuation in temperature. The temperature fluctuation, which contained higher harmonics, was generated experimentally by modulating the voltage across a stainless steel wire. Chemical conversion rates were detected by measuring the pressure changes induced by the non-equimolar oxidation reaction. Their work was limited by the lack of fundamental chemical and hydrodynamic models of their dynamic system and by difficulties associated with the mathematical analysis of a system response containing impure sinusoids.

Yasuda[72] recently extended his earlier studies of adsorption and diffusion to measurements of kinetic parameters of catalytic reactions within porous solids contained in flow reactors. He developed the mathematical framework and the experimental apparatus required to access kinetic processes with arbitrary kinetics. The apparatus consists of a flow reactor perturbed slightly in concentration by a two-piston system. Phase lags and amplitude changes were obtained by comparing the reactant and product concentrations at the reactor outlet using mass spectrometry. The frequency range was limited (< 0.2 Hz) and the only reported application is to the hydrogenation of propylene on supported Pt, a fairly simple and well-understood catalytic reaction. Analyses of the response data led to kinetic orders and rate constants that differed significantly from those reported in previous steady-state measurements on similar catalysts. In addition, the shape of the response curves could be described only by introducing a new type of pseudo-kinetic parameter reflecting the response of hydrogenation rates to changes in the derivative of the dihydrogen pressure, an unusual and previously unreported effect on reaction kinetic treatments.

Schrieffer and Sinfelt[94] have described a mathematical and conceptual framework for applications of FR methods to the measurement of the kinetics of adsorption-desorption and consecutive catalytic steps in flow reactors. In a very elegant treatment, they show how FR methods yield kinetic information not available from steady-state kinetic methods. Specifically, steady-state methods give rate constants that include both the intrinsic rate constant for the reaction of an intermediate and its surface concentration. The two components must be decoupled in order to calculate intrinsic rate constants (turnover rates), but this can only be done when independent measurements of surface concentrations are available. Instead, we often measure the number of certain types of surface sites by titration with probe molecules before catalytic reactions, and then assume that all sites are covered with reactive intermediates during catalysis.

FR methods preserve the steady-state and thus the identity and concentration of reaction intermediates while providing independent measures of both the intrinsic rate constant for a given site (turnover rate) and the surface concentration of the required reaction intermediates. It is, in theory, possible to identify the rate of kinetically distinct reaction steps within a catalytic sequence because the system response contains a frequency component that can access relaxation times of the several reaction steps. In spite of their obvious usefulness, these techniques have not been widely used to describe catalytic sequences. Isotopic jump techniques, on the other hand, which share some of the advantages of the FR methods have often been used in catalysis[97,98].

Finally, frequency-modulation techniques (modulated molecular beam relaxation)[37-40] have also been used in the analysis of surface reactions on oriented macroscopic single crystals. In these methods, a collimated molecular beam of chemically reactive components is directed at a reactive surface and then "chopped" by a rotating mask that produces square pulses of reactants within an ultrahigh vacuum background. Although not truly a steady-state technique, these molecular beam methods share much of their information content and mathematical framework with the FR methods discussed in our review.

3. Status and Trends

3.1 Experimental Methods

In Section 2.2, we mentioned several key challenges in the experimental application of FR techniques to the study of dynamic processes in gas-solid systems. Its use as a standard analytical probe of dynamic processes still requires significant improvements in the accuracy, time efficiency, and frequency range of the measurements.

We have recently designed a system that combines acoustically-coupled moving diaphragms capable of reaching higher forcing frequencies (150 Hz) with two synchronized and identical closed chambers, one containing the sample and the other an equivalent volume without a porous

solid sample (blank). This system extends the experimental frequency range well beyond those presently attainable (~10 Hz) and permits access to faster dynamic processes of special interest in the study of chemical reactions. It also allows substraction of the sample and blank response in real-time, a procedure that reduces significantly data acquisition requirements and the need to calculate amplitudes and phase lags from Fourier-Transform analyses of massive amounts of stored digital data. The real-time substraction is accomplished using integrated analog circuits that calculate amplitude attenuations and phase lags from direct comparisons of two electrical signals.

We are also exploring the use of more suitable forcing signals in order to decrease the experimental time required to obtain a response function over a wide range of frequency. Long experimental times are especially troublesome because small sample temperature variations can induce changes in pressure and in kinetic parameters similar in magnitude to those that we attempt to measure in the FR experiment. Sample contamination by background impurities in the system volume can also alter the adsorption and reactive properties of surfaces over extended periods of time. In order to minimize these effects, we are examining the use of forcing functions containing several superimposed sine waves of different frequency, as a method for probing the system response over many frequencies simultaneously. These signals containing multiple harmonic components (modulated frequency methods) have been suggested previously[99] but their feasibility awaits experimental demonstration.

Another more efficient FR method would use larger fluctuations (non-linear perturbations), which can change in amplitude between consecutive cycles (modulated amplitude FR). This can lead to simultaneous measurements of the system response at several concentrations of reacting or diffusing molecules. These methods increase the complexity of the mathematical analysis, by requiring the numerical solutions of the full constitutive equations. The benefits of linearized systems and the resulting compact expressions of the transfer functions in the frequency domain are no longer available, but the experimental times are markedly reduced.

3.2 Mathematical Analyses

An essential requirement in the interpretation of frequency response experiments is that the constitutive equations of the system must accurately describe its underlying physical and chemical mechanisms. This is crucial for the correct estimation of dynamic constants, pore volume, and adsorption capacities. In Section 2.3.1.2, we showed how the theoretical response functions based on a simple diffusion equation (Eqn. 7) could not explain the experimental FR data of certain gas-zeolite systems. A variety of diffusion mechanisms were proposed to describe the experimental observations, all of them were based on a single pore diffusion equation.

Interpretation of FR data requires modeling equations that account for all dynamic processes that respond to the applied perturbations. Besides intraparticle (mesoporous) or intracrystal (zeolite) phenomena, the FR of porous solids can be affected by other dynamic processes, whose net effect on the pressure response cannot generally be neglected. Notable among these are the dynamics and capacities of diffusion and adsorption processes of interparticle or intercrystal voids and of external mass transfer resistances. Some of these issues have been recently addressed by Jordi and Do[100]. These authors have theoretically examined the FR of diffusion and adsorption processes in bidisperse porous materials. They have shown that many subtle features of the response functions can be correctly described only by accounting for the coupling of adsorption, diffusion, and mass transfer mechanisms within these composite particles. Their work illustrates the importance of fundamental models, because seemingly similar response functions may reflect different dynamic mechanisms sharing similar relaxation times and reservoir capacities.

Currently, constitutive equations can be formulated with increasing levels of detail and their solution made possible by improved mathematical algorithms and by marked increases in computational storage and speed. Fundamental modeling equations, which are inherently non-linear, can therefore be solved numerically for any type of input perturbation. This provides incentives and a mechanism for exploring the FR of systems subject to large amplitude perturbations that no longer need to be restricted to simple harmonic functions. Clearly, this approach does not benefit from the elegant treatments available for linearized equations, but offers instead significant advantages of time efficiency by allowing the scoping of a range of frequencies and amplitudes simultaneously.

We have, for example, numerically solved Eqns. (13)-(17) for a variety of input perturbations. When the input is a sinusoid of small amplitude, we recover the results of the analytical transfer function [Eqn. (18)] exactly. By gradually increasing the amplitude of the sine perturbation, we quantitatively establish the validity of the analytical linear solution of the FR equations. More importantly, we have also obtained non-linear pressure response functions for the mesoporous system subjected to heavily damped oscillations and to simultaneous sinusoids of varying frequency and amplitude. We are currently using these results to design a more efficient FR apparatus that can speed up the process of obtaining dynamic parameters in porous catalytic solids.

3.3 Chemical Reactions

The potential of FR methods in the analysis of the dynamics of complex catalytic sequences remains unexploited[94], a result of historical experimental and theoretical hurdles that have been mostly overcome today. Highly accurate electronic flow controllers with fast response are now

readily available and can be used to introduce small perturbations in either concentration or isotopic content into a flowing stream. Mass spectrometry has evolved into a rapid analysis technique with improved mass resolution and response time. The mathematics required for analysis of the response functions and the fundamental kinetic models describing individual steps in catalytic sequences have also evolved markedly in both generality and sophistication. Two types of FR methods remain largely unexplored for the analysis of chemical reactions: frequency-modulated isotopic switch techniques and measurements of transfer rates at equilibrium by volume modulation of a closed (non-equimolar) reaction system.

In the first, the limitation of isotopic switch techniques in the deconvolution of multiple kinetic steps and pools of surface intermediates is overcome by introducing isotopic jumps with varying time delays between them. These systems can be analyzed using Fourier-Transform methods similar to those applied in pulse and modulated beam studies. The delay between isotopic switches allows pools of surface intermediates and kinetic processes with different characteristic lifetimes and reaction times to be accessed selectively during a single series of experiments. This technique avoids the ill-posed deconvolution of individual exponential terms within a sum, which currently limit the information available from single isotopic switch methods.

The other application involves the measurement of a reaction rate near its chemical equilibrium by introducing a small perturbation in the volume of a closed system. For non-equimolar reactions, the resulting change in pressure shifts the chemical equilibrium of the chemical reaction, and the system responds with a small net reaction rate in the restoring direction characterized by a reaction relaxation time[55,56]. Near equilibrium, reaction rates become proportional to the affinity of the reaction mixture, defined as the difference in chemical potential between the mixture and its equilibrium composition. By varying the magnitude perturbation from equilibrium (within the linear range), one obtains the dependence of the restoring or transfer rate on the reaction affinity, the slope of which reflects the stoichiometric number of the rate-determining step[101,102], which reflects the number of times that such a step must occur in order for the catalytic sequence to turn over once. Often, these measurements are the only recourse available in order to distinguish among several possible reaction mechanisms and potential rate-determining steps[103]. The mathematical analyses of the FR of non-equimolar reactions in closed systems requires only a simple extension of our treatment in Section 2.3.2 and the Appendix.

4. Acknowledgements

We acknowledge the expert technical contributions of Messrs. G. J. DeMartin and R. H. Ernst and of Dr. C. P. Kelkar to our experimental FR studies. We also thank Dr. B. S. White for providing valuable guidance in the use of mathematical perturbation techniques. Finally, we thank

Dr. John H. Sinfelt for many rewarding discussions and for his continuous encouragement during the course of these studies.

5. Nomenclature

A_{ij}	components of matrix $\underline{\underline{A}}$ defined in Eqns. (A15)-(A18)
C	average molar concentration within porous material
C_n	molar gas phase concentration within pore voids (e: equilibrium)
$\hat{C}_n$	relative time-dependent amplitude change in C_n
$\overline{C}_n$	relative time-independent amplitude change in C_n
D	average Fickian diffusivity within porous material
d_n	effective surface diffusivity of adsorbed species n
D_n	effective void diffusivity of gaseous species n
E_n	dimensionless variable defined in Eqn. (A24)
f	effectiveness factor function (see Eqns. (A26)-(A29))
F_n	dimensionless variable defined in Eqn. (A25)
$H(i\omega)$	complex transfer function
$\|\|H(i\omega)\|\|$	magnitude of transfer function (see Eqn. 19)
i	imaginary number ($i^2 = -1$)
I_o	modified Bessel function of order zero
I_1	modified Bessel function of order one
$Im(H)$	imaginary component of transfer function H
J_o	Bessel function of order zero
K	dimensionless capacity defined in Eqn.(4)
K_j, K_{-j}	kinetic parameters defined in Eqn.(3)
k_{aj}	Langmuir adsorption constant for species j
k_{dj}	Langmuir desorption constant for species j
$K_{n\ell}$	equilibrium adsorption constant of species n on sites of type ℓ
$k_{an\ell}$	adsorption constant of species n on sites of type ℓ
$k_{dn\ell}$	desorption constant of species n on sites of type ℓ
L	number of types of active sites
L_o	length of cylindrical particle
M	total number of species in gaseous mixture
M_w	diffusant molecular weight
N	molar adsorption capacity of porous material
n_v	total number of moles contained within intraparticle pore volume V_p
p	relative pressure amplitude
$P(t)$	total pressure within batch system
P_e	equilibrium pressure
P_n	partial pressure of species n within the system volume (e: equilibrium)
$\hat{P}_n$	relative time-dependent amplitude change in P_n
$\overline{P}_n$	relative time-independent amplitude change in P_n
$\underline{\underline{P}}$	matrix of normalized eigenvectors of $\underline{\underline{A}}$

$\underline{\underline{Q}}$	inverse matrix of $\underline{\underline{P}}$
r	radial coordinate in porous particle
R	universal gas constant
R_j	net adsorption rate of species j
r_o	characteristic particle dimension
Re(H)	real component of transfer function H
s	geometric factor (s=1 slab, s=2 cylinder, s=3 sphere)
S_n	molar concentration of adsorbed species n (e: equilibrium)
$\hat{S}_n$	relative time-dependent amplitude change in S_n
$\overline{S}_n$	relative time-independent amplitude change in S_n
t	time
T	absolute temperature
U_n	dimensionless variable defined in Eqn. (A10)
v	relative volume amplitude
V	volume of batch system excluding volume of particles (e: equilibrium)
$\hat{V}$	relative time-dependent amplitude change in V
$\overline{V}$	relative time-independent amplitude change in V
V_n	equivalent volume of adsorbed phase defined in Eqn. (A8)
V_p	intraparticle pore volume of mesoporous structure
W_n	dimensionless variable defined in Eqn. (A10)
$\underline{x}$	vector of dimensionless variables (see Eqn. (A19))
y_n	equilibrium molar fraction of species n within batch system
$\underline{z}$	vector of dimensionless variables (see Eqn. (A21))

Greek Symbols

α	exponent of kinetic equation for adsorption
β_n	dimensionless parameter defined in Eqn. (A8)
γ_i	zeroes of Bessel function $J_o(\gamma_i)=0$
∇	Laplacian operator in slab, cylindrical, or spherical geometry
ε	small perturbation parameter
η	dimensionless frequency defined in Eqn.(12)
λ	dimensionless variable defined in Eqn.(23)
$\underline{\underline{\Lambda}}$	diagonal matrix containing the eigenvalues of matrix $\underline{\underline{A}}$
ξ	dimensionless coordinate in porous particle
ρ_p	particle density
ν_i	auxiliary variable defined as $\nu_i^2 = \gamma_i^2 + \psi_m^2$
ϕ	phase lag between volume and pressure signals
ψ_m^2	mth eigenvalue of matrix $\underline{\underline{A}}$
ω	modulating frequency

6. Appendix

Here we derive analytical transfer functions that describe the FR of the conservation equations derived in Section 2.3.2 (Eqns. (13)-(17)). The first step in the analysis is to express the volume of the system in terms of a small perturbation parameter ε:

$$V = V_e(1-\varepsilon\hat{V}), \tag{A1}$$

where $\hat{V}$ is an arbitrary amplitude change later defined as a harmonic perturbation. The change in V induces changes in pressure and concentration (gas and surface) for each species in the system:

$$C_n = C_{ne}(1+\varepsilon\hat{C}_n); \quad S_n = S_{ne}(1+\varepsilon\hat{S}_n); \quad P_n = P_{ne}(1+\varepsilon\hat{P}_n) \tag{A2}$$

Substituting Eqn. (A2) into Eqns. (13)-(17) and retaining terms of order ε only, leads to a linear system of partial differential equations:

$$\frac{\partial\hat{C}_n}{\partial t} = D_n\nabla^2\hat{C}_n - \frac{\rho_p}{C_{ne}}\sum_{\ell=1}^{L} k_{dn\ell}S_{ne}^{\alpha}[\hat{C}_n - (\frac{\alpha}{1-S_{ne}/N})\hat{S}_n] \tag{A3}$$

$$\hat{C}_n(r_o,t) = \hat{P}_n(t); \quad \frac{\partial\hat{C}_n}{\partial r}(0,t) = 0; \quad \hat{C}_n(r,0) = 0 \tag{A4}$$

$$\frac{\partial\hat{S}_n}{\partial t} = d_n\nabla^2\hat{S}_n + \frac{1}{S_{ne}}\sum_{\ell=1}^{L} k_{dn\ell}S_{nc}^{\alpha}[\hat{C}_n - (\frac{\alpha}{1-S_{ne}/N})\hat{S}_n] \tag{A5}$$

$$\hat{S}_n(r_o,t) = \beta_n\hat{C}_n(r_o,t); \quad \frac{\partial\hat{S}_n}{\partial r}(0,t) = 0; \quad \hat{S}_n(r,0) = 0 \tag{A6}$$

$$\hat{P}_n(t) = \hat{V} - \int_o^{r_o}\frac{sr^{s-1}}{r_o^s}\left(\frac{V_p}{V_e}\hat{C}_n + \frac{V_n}{V_e}\hat{S}_n\right)dr, \tag{A7}$$

where

$$\beta_n = \frac{(K_{n\ell}C_{ne})^{(\alpha-1)/2}}{\alpha[1+(K_{n\ell}C_{ne})^{(\alpha+1)/2}]}; \qquad V_n = S_{ne}RT/P_{ne} \tag{A8}$$

β_n measures the change in surface concentration driven by a change in gas concentration. V_n is the adsorption capacity of the solid for species n, expressed as an equivalent volume at pressure

P_{ne} and temperature T. In Eqns. (A3)-(A8) we have assumed conditions of low surface coverages where the term ($N-\Sigma S_j$) can be replaced by ($N-S_n$) without significant error for multicomponent systems and being exact for simple species analysis.

Eqns. (A3)-(A8) describe the time-dependent amplitude changes in pressure ($\hat{P}_n$) and concentration ($\hat{C}_n, \hat{S}_n$), driven by changes in the system volume ($\hat{V}$), for any type of input perturbation. For harmonic perturbations, the respective amplitudes can be expressed as:

$$\hat{V} = \overline{V}\, e^{i\omega t}\ ; \quad \hat{C}_n = \overline{C}\, e^{i\omega t}\ ; \quad \hat{S}_n = \overline{S}_n\, e^{i\omega t}\ ; \quad \hat{P}_n = \overline{P}_n\, e^{i\omega t} \tag{A9}$$

Substituting Eqn. (A9) into Eqns. (A3)-(A8), and defining

$$\xi = \frac{r}{r_o}; \quad U_n = \frac{\overline{C}_n}{\overline{P}_n}; \quad W_n = \frac{\overline{S}_n}{\beta_n \overline{P}_n}\ , \tag{A10}$$

leads to the following linear system of boundary value problems in the frequency domain:

$$\nabla^2 U_n = A_{n,n} U_n + A_{n,M+n} W_n \tag{A11}$$

$$\nabla^2 W_n = A_{M+n,n} U_n + A_{M+n,M+n} W_n \tag{A12}$$

$$U_n(1) = W_n(1) = 1; \quad \frac{\partial U_n}{\partial \xi}(0) = \frac{\partial W_n}{\partial \xi}(0) = 0 \tag{A13}$$

$$\frac{\overline{P}_n}{\overline{V}} = \frac{1}{1 + \int_o^1 s\xi^{s-1}\left(\frac{V_p}{V_c} U_n + \frac{V_n}{V_e}\beta_n W_n\right) d\xi}\ , \tag{A14}$$

where

$$A_{n,n} = \frac{i\omega r_o^2}{D_n} + \left(\frac{\rho_p r_o^2 S_{ne}^{\alpha}}{D_n C_{ne}}\right)\sum_{\ell=1}^{L} k_{dn\ell} \tag{A15}$$

$$A_{n,M+n} = -\left(\frac{\rho_p r_o^2 S_{ne}^{\alpha}\beta_n \alpha}{D_n C_{ne}(1 - S_{ne}/N)}\right)\sum_{\ell=1}^{L} k_{dn\ell} \tag{A16}$$

$$A_{M+n,n} = -\left(\frac{r_o^2 S_{ne}^{\alpha-1}}{d_n \beta_n}\right)\sum_{\ell=1}^{L} k_{dn\ell} \tag{A17}$$

$$A_{M+n,M+n} = \frac{i\omega r_o^2}{d_n} + \left(\frac{\alpha r_o^2 S_{ne}^{\alpha-1}}{d_n(1 - S_{ne}/N)} \right) \sum_{\ell=1}^{L} k_{dn\ell} \tag{A18}$$

The solution of Eqns. (A11)-(A13) for U_n and W_n and their substitution into Eqn. (A14) directly gives the pressure response of species n ($\overline{P}_n$) to a volume change ($\overline{V}$) in the system, i.e., the transfer function of species n in the FR experiment. Its solution is easily obtained in closed-form for slab, cylindrical, or spherical geometries. The first step is to recast the equations in matrix form:

$$\nabla^2 \underline{x} = \underline{\underline{A}}\underline{x}, \quad \underline{x} = [U_1,....,U_M, W_1,...,W_M]^T \tag{A19}$$

$$\underline{x}(1) = [1,....,1]^T, \quad \frac{\partial \underline{x}}{\partial \xi}(0) = [0,....,0]^T, \tag{A20}$$

where the only non-zero matrix elements in $\underline{\underline{A}}$ are those defined in Eqns. (A15)-(A18). The matrix Eqn. (A19) can be made diagonal by the transformation $\underline{x} = \underline{\underline{P}}\underline{z}$, where $\underline{\underline{P}}$ is the matrix of the normalized eigenvectors of $\underline{\underline{A}}$. Substituting that transformation into Eqn. (A19) after pre-multiplying by a matrix $\underline{\underline{Q}}$ (where $\underline{\underline{Q}}$ is the inverse matrix of $\underline{\underline{P}}$) leads to:

$$\nabla^2 \underline{z} = \underline{\underline{\Lambda}}\underline{z}, \quad \underline{z} = [z_1,...,z_{2M}]^T \tag{A21}$$

$$\underline{z}(1) = \underline{\underline{Q}}\underline{x}(1), \quad \frac{\partial \underline{z}}{\partial \xi}(0) = [0,....,0]^T \tag{A22}$$

$\underline{\underline{\Lambda}}$ is a diagonal matrix with diagonal elements given by the eigenvalues of $\underline{\underline{A}}$. These equations are then solved for a given pellet geometry and their solution is substituted into Eqn. (A14) to obtain an analytic transfer function H for species n:

$$H = \frac{\overline{P}_n}{\overline{V}} = \frac{1}{1 + \frac{V_p}{V_e} E_n + \frac{V_n}{V_e} F_n}, \tag{A23}$$

where

$$E_n = \sum_{m=1}^{2M} P_{n,m} \left(\sum_{k=1}^{2M} Q_{m,k} \right) f(\psi_m) \tag{A24}$$

$$F_n = \beta_n \sum_{m=1}^{2M} P_{M+n,m} \left(\sum_{k=1}^{2M} Q_{m,k} \right) f(\psi_m) \tag{A25}$$

$$f(\psi_m) = \tanh \psi_m / \psi_m \qquad \text{(slabs)} \tag{A26}$$

$$= \frac{2I_1(\psi_m)}{\psi_m I_0(\psi_m)} \qquad \text{(long cylinders)} \tag{A27}$$

$$= \frac{2I_1(\psi_m)}{\psi_m I_0(\psi_m)} + \frac{r_o}{L_o} \sum_{i=1}^{\infty} \frac{8\psi_m^2}{\upsilon_i^3 \gamma_i^2} (1 - e^{-\upsilon_i L_o / r_o}) \qquad \text{(short cylinders)} \tag{A28}$$

$$= \frac{3}{\psi_m} (\coth \psi_m - \frac{1}{\psi_m}) \qquad \text{(spheres)} \tag{A29}$$

In the above equations, ψ_m^2, is the mth eigenvalue of the matrix $\underline{\underline{A}}$, I_n is the modified Bessel function of order n, γ_i is the ith zero of the Bessel function $J_0(\gamma_i)=0$, $\upsilon_i^2 = \gamma_i^2 + \psi_m^2$, and L_o is the length of the cylinder. The solution for short cylinders was obtained by Ho and Hsiao[104] and accounts for additional diffusion processes occurring through the ends of the cylinder when L_o/r_o is not very large.

For a system of M species that diffuse and adsorb independently of each other (Knudsen diffusion regime), the global transfer function takes the form:

$$H(i\omega) = \sum_{n=1}^{M} \left(\frac{y_n}{1 + \frac{V_p}{V_e} E_n + \frac{V_n}{V_e} F_n} \right). \tag{A30}$$

where y_n is the molar fraction of species n within the system. This equation describes the pressure response of the system to an applied volume perturbation. H is a complex function containing real and imaginary components (phase lag) and its magnitude is always lower or equal than one (amplitude attenuation). It is composed of the sum of the responses of the individual species because under a Knudsen diffusion regime molecules do not interact within the solid voids. The individual responses contain two coupled dynamic terms (E_n and F_n) that account for the dynamics of the diffusion and adsorption processes within the intraparticle pore volume of mesoporous structures. The capacities associated with these dynamic processes in the pore voids and the adsorbed phase are given by V_p/V_e and V_n/V_e, respectively.

7. References

1. J.O. Hougen, Chem. Eng. Progr. Monograph Ser. No. 4, Vol. 60, 1964.
2. A.J. Angstrom, Ann. Phys. Chem., 1861, 114, 513-530.
3. S.K. Evnochides and E.J. Henley, J. Polym. Sci., 1970, 8, 1987-1997.
4. K. Sekine, Chem. Lett. (Chemical Society of Japan) , 1975, 8, 841-846.
5. Z.T. Fattakhova, Y.A. Frank, and A.D. Berman, Kinet. Kataliz. , 1978, 19, 489-494.
6. R.R. Goddard, Soc. Petr. Eng. J., 1966, 6, 143-152.
7. E. Charlaix, A.P. Kushnick, and J.P. Stokes, Phys. Rev. Lett., 1988, 61, 1595-1598.
8. J.B. Rosen and W.E. Winsche, J. Chem. Phys., 1950, 18, 1587-1592.
9. S. Whitaker and R. L. Pigford, AIChE J., 1966, 12, 741-746.
10. K.H. Lee and T.Z. Fahidy, Instruments and Control Systems, 1967, 40, 141-143.
11. G.G. Pollock and A.I. Johnson, Can. J. Chem. Eng., 1969, 47, 565-575.
12. G.G. Pollock and A.I. Johnson, Can. J. Chem. Eng., 1970, 48, 711-719.
13. S.S.E.H. El-Nashaie, M.A. El-Rifai, and M.N. Abd El-Hakim, Chem.Engng. Sci., 1978, 33, 847-852.
14. P. Moravec and V. Stanēk, Chem. Eng. Process., 1988, 24, 93-103.
15. P.F. Deisler, Jr. and R.H. Wilhelm, Ind. Engng. Chem., 1953, 45, 1219-1227.
16. H. Kramers and G. Alberda, Chem. Engng. Sci., 1953, 2, 173-181.
17. K.W. McHenry, Jr. and R.H. Wilhelm, AIChE J. , 1957, 3, 83-91.
18. G.A. Turner, Chem. Engng. Sci. , 1959, 10, 14-21.
19. D.E. Bidstrup, Ph.D. Thesis, Ohio State University, 1966.
20. G.A. Turner, AIChE J., 1967, 13, 678-682.
21. D.J. Gunn, Chem. Engng. Sci., 1970, 25, 53-66.
22. J. Sinai and A.S. Foss, AIChE J., 1970, 16, 658-669.
23. D.J. Gunn and R. England, Chem. Engng. Sci., 1971, 26, 1413-1423.
24. J.D. Tinkler and D.E. Lamb, Chem. Eng. Progr. Symp. Series, 1965, 61, 155-167.
25. F. Leder and J.B. Butt, AIChE J., 1966, 12, 1057-1063.
26. J.E. Crider and A.S. Foss, AIChE J., 1968, 14, 77-84.
27. J.A. Hoiberg, B.C. Lyche, and A.S. Foss, AIChE J., 1971, 17, 1434-1447.
28. H. Kumazawa and N. Morita, J. Chem. Eng. Jpn, 1971, 4, 269-274.
29. C.-C. Chen and J.C. Friedly, Ind. Eng. Chem. Fundam., 1974, 13, 121-126.
30. D.T. Lynch and N.P. Walters, Chem. Engng. Sci., 1990, 45, 1089-1096.
31. J.M. Douglas, Ind. Engng. Chem. Process Des. Dev., 1967, 6, 43-48.
32. F.E. Gore, Ind. Eng. Chem. Process Des. Dev. 1967, 6 (1), 10-16.
33. A.B. Ritter and J.M. Douglas, Ind. Eng.Chem. Fundam., 1970, 9, 21-28.
34. J.L. Feimer, P.L. Silveston, and R.R. Hudgins, Can. J. Chem. Engng., 1985, 63, 86-92.
35. T.Z. Fahidy and D.D. Perlmutter, Can. J. Chem. Eng. , 1966, 44, 95-99.
36. R.H. Jones, D.R. Olander, W. J. Siekhaus, and J.A. Schwarz, J. Vac. Sci. Technol., 1972, 9, 1429-1441.
37. J.A. Schwarz and R.J. Madix, Surface Sci., 1974, 46, 317-341.
38. H.-C. Chang and W.H. Weinberg, Surface Sci., 1977, 65, 153-164.
39. H.-C. Chang and W.H. Weinberg, Surface Sci. ,1978, 72, 617-634.

40. J.R. Engstrom and W.H. Weinberg, Surface Sci., 1988, 201, 145-170.
41. H.H. Shugart, Jr., D.E. Reichle, N.T. Edwards, and J.R. Kercher, Ecology, 1976, 57, 99-109.
42. F. Vardar and M.D. Lilly, Biotechnol. Bioeng. , 1982, 24, 1711-719.
43. R.L. Dwyer and K.T. Perez, American Naturalist, 1983, 121, 305-323.
44. W.D. Nicholas and A.R. Abernathy, Chemosphere , 1987, 16, 287-295.
45. A.E. Weber and K.-Y. San, Biotechnol. Bioeng., 1989, 34, 1104-1113.
46. J.W. Blackburn, Ann. New York Acad. Sci. , 1990, 589, 580-592.
47. J.G. Lazar and J. Ross, Science, 1990, 247, 189-192.
48. W.C. Clements, Jr. and K.B. Schnelle, Jr., Ind. Eng. Chem. Process Des. Dev., 1963, 2, 94-102.
49. V.J. Law and R.V. Bailey, Chem. Engng. Sci., 1963, 18, 189-202.
50. J.R. Hays, K.B. Schnelle, and P.A. Frenkel, Eng. Ext. Ser., 1964, 117, 777-795.
51. J.L. Johnson, L.T. Fan, and Y.-S. Wu, Ind. Eng. Chem. Process Des. Develop., 1971, 10, 425-431.
52. W.C. Clements, Jr., Ind. Eng. Chem. Process Des. Develop., 1972, 11, 461-462.
53. V.F. Smolen, Kinet. Data Anal. (Proc. Satell. Symp.), 1981, pp. 209-233.
54. P.K. Sarkar, B. Rakshit, D. Mukhopadhyay, and R.N. Mukherjea, J. Inst. Eng., 1986, 67, 17-26.
55. M. Eigen, Discuss. Faraday Soc., 1954, 17, 194-205.
56. M. Eigen and L. de Maeyer, "Technique of Organic Chemistry", Vol. VIII-Part II. Rates and Mechanisms of Reactions, 2nd ed.; (Weissberger, A., ed.). Interscience Publishers: London, 1963, pp. 895-1054.
57. H.M. Hulburt and Y.G. Kim, Ind. Eng. Chem., 1966, 58(9), 20-31.
58. R.W. Arbesman and Y.G. Kim, Ind. Eng. Chem. Fundam. , 1969, 8, 216-221.
59. M.I. Temkin,, Kinetika i Kataliz, 1976, 17, 1095-1099.
60. L.M. Naphtali and L.M. Polinski, , J. Phys. Chem., 1963, 67, 369-375.
61. L. Polinski and L. Naphtali, Adv. Catal., 1969, 19, 241-291.
62. Y. Yasuda, J. Phys. Chem., 1976, 80, 1867-1869.
63. Y. Yasuda, J. Phys. Chem., 1976, 80, 1870-1875.
64. Y. Yasuda and M. Saeki, J. Phys. Chem., 1978, 82, 74-80.
65. Y. Yasuda, J. Phys. Chem., 1982, 86, 1913-1917.
66. Y. Yasuda and G. Sugasawa, J. Phys. Chem., 1982, 86, 4786-4791.
67. Y. Yasuda and G. Sugasawa, J. Catal., 1984, 88, 530-534.
68. Y. Yasuda and A. Yamamoto, J. Catal., 1985, 93, 176-181.
69. Y. Yasuda, Y. Yamada, and I. Matsuura, Stud. Surf. Sci. Catal., 1986, 28, 587-594.
70. Y. Yasuda and S. Shinbo, Bull. Chem. Soc. Jpn., 1988, 61, 745-751.
71. Y. Yasuda and K. Matsumoto, J. Phys. Chem., 1989, 93, 3195-3200.
72. Y. Yasuda, J. Phys. Chem., 1989, 93, 7185-7190.
73. Y. Yasuda, Y. Suzuki, and H. Fukada, J. Phys. Chem., 1991, 95, 2486-2492.
74. Y. Yasuda, Bull. Chem. Soc. Jpn., 1991, 64, 954-961.
75. L.V.C. Rees, "Structure and Reactivity of Modified Zeolites" (P. A. Jacobs et al., eds.), Elsevier Science Publishers: Amsterdam, 1984, pp 1-11.
76. M. Bülow, H. Schlodder, L.V.C. Rees, and R.E. Richards, Stud. Surf. Sci. Catal., 1986, 28, 579-586.

77. N.G. Van-den-Begin and L.V.C. Rees, "Zeolites: Facts, Figures, Future" (P. A. Jacobs and R. A. van Santen, eds.), Elsevier Science Publishers: Amsterdam, 1989, pp. 915-924.
78. N. Van-den-Begin, L.V.C. Rees, J. Caro, M. Bülow, M. Hunger, and J. Kärger, J. Chem. Soc., Faraday Trans. 1, 1989, 85, 1501-1509
79. L.V.C. Rees and D. Shen, J. Chem. Soc. Faraday Trans. , 1990, 86, 3687-3692.
80. N. Van-den-Begin, Ph.D. Thesis, University of London, 1990.
81. D. Shen and L.V.C. Rees, Zeolites, 1991, 11, 684-689.
82. D. Shen and L.V.C. Rees, Zeolites, 1991, 11, 666-671.
83. D. Shen and L.V.C. Rees, 9th International Symp. on Catalysis, Paper B12, 1992.
84. G. Marcelin, J.E. Lester, S.C. Chuang, and J.G. Goodwin, Jr., Proc. of 9th Iberoam. Symp. Catal., Vol. 1, 1984, pp. 271-280.
85. J.G. Goodwin, Jr., A. Sayari, J.E. Lester, and G. Marcelin, Am. Chem. Soc., Div. Pet. Chem., 1984, 29, 690-698.
86. J.G. Goodwin, Jr., J.E. Lester, G. Marcelin, and S.F. Mitchell, ACS Symp. Series, 1985, 288, 67-78.
87. G. Marcelin, J.E. Lester, and S.F. Mitchell, J. Catal., 1986, 102, 240-248.
88. Y.-E. Li and R.D. Gonzalez, Proc. of 11th Iberoam. Symp. Catal., Vol. 1, 1988, pp. 33-39.
89. Y.-E. Li, D. Willcox, and R.D. Gonzalez, AIChE J. , 1989, 35, 423-428.
90. S.C. Reyes, G.J. DeMartin, C.P. Kelkar, R.H. Ernst, and E. Iglesia, ACS Meeting on Chemistry and Characterization of Supported Metal Catalysts, August 22-27, Chicago, IL.
91. C.I. Rutherford, Proc. Inst. Mech. Engrs. (London), 1950, 162, 334-343.
92. D.R. Coughanowr and L.B. Koppel, "Process Systems Analysis and Control". McGraw-Hill, New York, pp. 211-276 (1965).
93. G. Stephanopoulous, "Chemical Process Control". Prentice Hall, Englewood, NJ, pp. 317-343 (1984).
94. J.R. Schrieffer and J.H. Sinfelt, J. Phys. Chem., 1990, 94, 1047-1050.
95. A.L. Dent and R.J. Kokes, J. Phys. Chem., 1969, 73, 3781-3790.
96. S.C. Reyes and E. Iglesia, J. Catal., 1991, 129, 457-472.
97. J. Happel, "Isotopic Assessment of Heterogeneous Catalysis". Academic Press, FL (1986).
98. A. Ozaki, "Isotopic Studies of Heterogeneous Catalysis". Academic Press, NY (1977).
99. B.F. Cusset and D.A. Mellichamp, Ind. Eng. Chem. Process Des. Dev., 1975, 14, 359-368.
100. R.G. Jordi and D.D. Do, Chem. Engng. Sci., (in press).
101. Y. Kaneko and S. Oki, J. Res. Inst. Catalysis, 1967, 15, 185-192.
102. C.A. Hollingsworth, J. Chem. Phys., 1957, 27, 1346-1348.
103. M. Boudart and G. Djega-Mariadassou, "Kinetics of Heterogeneous Catalytic Reactions". Princeton University Press, NJ (1984).
104. T.C. Ho and G.C. Hsiao, Chem. Engng. Sci. , 1977, 32, 63-66.

Table 1. Some representative uses of FR techniques in the analysis of chemical and transport processes.

Application	Authors	Reference
1. Thermal Conductivity of Solids	Angstrom (1861)	2
2. Diffusivities in Polymers, Metals, and Solids	Evchnochides and Henley (1970)	3
	Sekine (1975)	4
	Fattakhova et al. (1978)	5
3. Dispersion and Permeability in Porous Media	Goddard (1966)	6
	Charlaix et al. (1988)	7
4. Dynamics of Chromatographic, Absorption, Extraction, and Backmixed Processes	Rosen and Winsche (1950)	8
	Whitaker and Pigford (1966)	9
	Lee and Fahidy (1967)	10
	Pollock and Johnson (1969,1970)	11,12
	El-Nashaie et al. (1978)	13
	Moravec and Stanek (1988)	14
5. Diffusion and Dispersion in Packed Beds	Deisler and Wilhelm (1953)	15
	Kramers and Alberda (1953)	16
	McHenry and Wilhelm (1957)	17
	Turner (1959)	18
	Bidstrup (1966)	19
	Turner (1967)	20
	Gunn (1970)	21
	Sinai and Foss (1970)	22
	Gunn and England (1971)	23
6. Chemical Reactions in Packed-Beds	Tinkler and Lamb (1965)	24
	Leder and Butt (1966)	25
	Crider and Foss (1968)	26
	Hoiberg et al. (1971)	27
	Kumazawa and Morita (1971)	28
	Chen and Friedly (1974)	29
	Lynch and Walters (1990)	30

Table 1 (cont'd.)

Application	Authors	Reference
7. Periodic Operation of Reactors	Douglas (1967)	31
	Gore (1967)	32
	Ritter and Douglas (1970)	33
	Feimer et al. (1985)	34
8. Dynamics of Surface Reactions	Fahidy and Perlmutter (1966)	35
	Jones et al. (1972)	36
	Schwarz and Madix (1974)	37
	Chang and Weinberg (1977,1978)	38,39
	Engstrom and Weinberg (1988)	40
9. Dynamic Processes in Biochemical Systems	Shugart et al. (1976)	41
	Vardar and Lilly (1982)	42
	Dwyer and Perez (1983)	43
	Nicholas and Abernathy (1987)	44
	Weber and San (1989)	45
	Blackburn (1990)	46
	Lazar and Ross (1990)	47
10. FR Analysis of Pulse Techniques	Clements and Schnelle (1963)	48
	Law and Bailey (1963)	49
	Hays et al. (1964)	50
	Johnson et al. (1971)	51
	Clements (1972)	52
	Smolen (1981)	53
	Sarkar et al. (1986)	54
11. Relaxation Methods in Chemical Kinetics	Eigen (1954)	55
	Eigen and deMaeyer (1963)	56
	Hulburt and Kim (1966)	57
	Arbesman and Kim (1969)	58
	Temkin (1976)	59

Figure Legends

Figure 1 In-phase and out-of-phase components of FR. Adsorption-desorption of a single species (Eqns. 1 and 2).

Figure 2 In-phase and out-of-phase components of FR. Diffusion in spherical particles (Eqns. 9 and 11).

Figure 3 Amplitude ratio (p/v) and phase lag (ϕ) as a function of dimensionless frequency ω/K_j (Bode diagram, Eqns. 19 and 20). Adsorption-desorption of a single species.

Figure 4 Amplitude ratio (p/v) and phase lag (ϕ) as a function of dimensionless frequency η (Bode diagram, Eqns. 19 and 20). Diffusion in spherical particles.

Figure 5 Out-of-phase components of FR. Hydrogen adsorption on Ni catalyst at 590 K. (After Naphtali and Polinski[60,61])

Figure 6 In-phase components of FR. Hydrogen adsorption on ZnO at 253 K (o: 0.021 Torr, •: 0.020 Torr). (After Yasuda[63])

Figure 7 Out-of-phase components of FR. Hydrogen adsorption on ZnO at 253 K (o: 0.021 Torr, •: 0.020 Torr). (After Yasuda[63])

Figure 8 Adsorption isotherm of hydrogen on ZnO at 253 K. (After Yasuda[63])

Figure 9 Out-of-phase components of FR. Chemisorption of hydrogen on supported Rh at 433 K and 0.5 Torr. (After Marcelin et al.[87])

Figure 10 Experimental values of the tangent of the phase lag ϕ as a function of forcing frequency (A: 429K, B: 343K). (After Li et al.[89])

Figure 11 Amplitude ratio as a function of dimensionless frequency. Diffusion of ethane in polyethylene films. (After Evnochides and Henley[3])

Figure 12 Phase lag as a function of dimensionless frequency. Diffusion of ethane in polyethylene films. (After Evnochides and Henley[3])

Figure 13 FR of Kr diffusion in Na-mordenite at 253 K and 1 Torr. (After Yasuda[65])

Figure 14 FR of Kr diffusion in zeolite A at 195 K and 5.8 Torr. (After Yasuda and Sagasawa[67])

Figure 15 Fickian diffusivities of light hydrocarbons as a function of temperature determined by various methods (o:CH_4, □:C_2H_6, Δ :C_3H_8). (After Yasuda et al.[73])

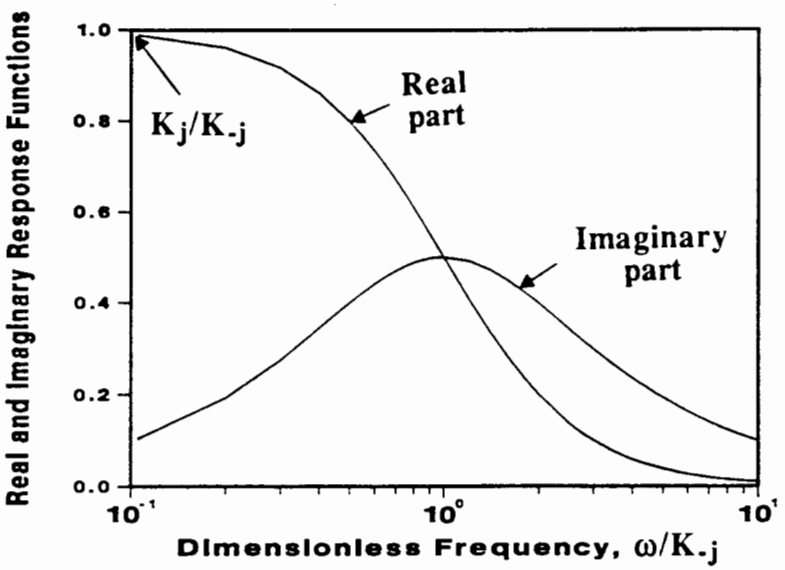
Real and Imaginary Response Functions
1.0
0.8
0.6
0.4
0.2
0.0
10^{-1}
10^{0}
10^{1}
K_j/K_{-j}
Real part
Imaginary part
Dimensionless Frequency, ω/K_{-j}

Figure 1

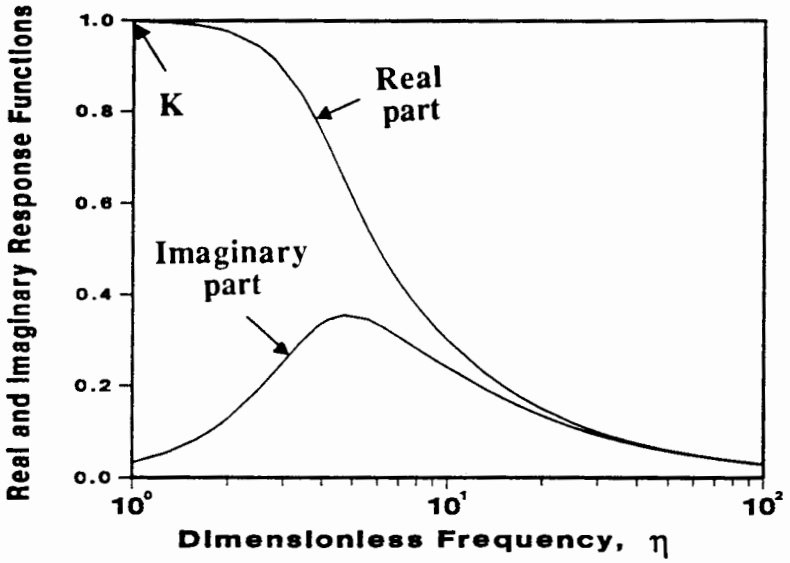
Real and Imaginary Response Functions
1.0
0.8
0.6
0.4
0.2
0.0
K
Real part
Imaginary part
10°
10¹
10²
Dimensionless Frequency, η

Figure 2

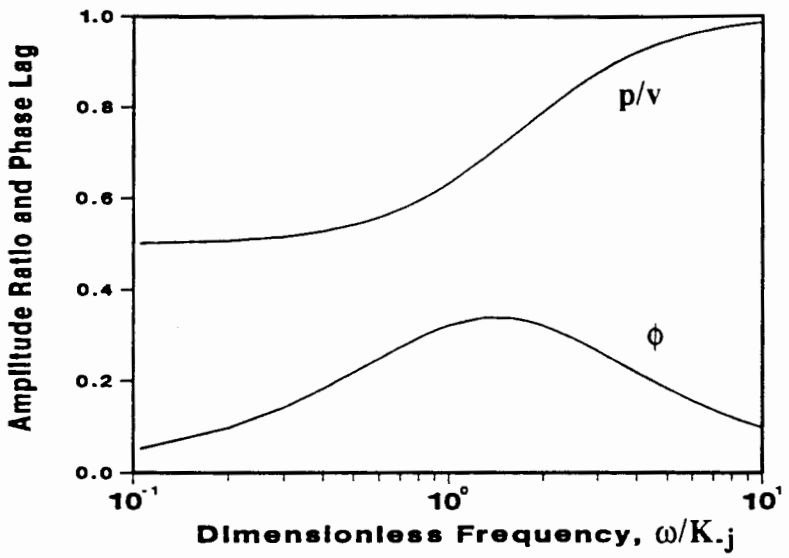
Amplitude Ratio and Phase Lag
1.0
0.8
0.6
0.4
0.2
0.0
p/v
ϕ
10⁻¹
10⁰
10¹
Dimensionless Frequency, ω/K.j

Figure 3

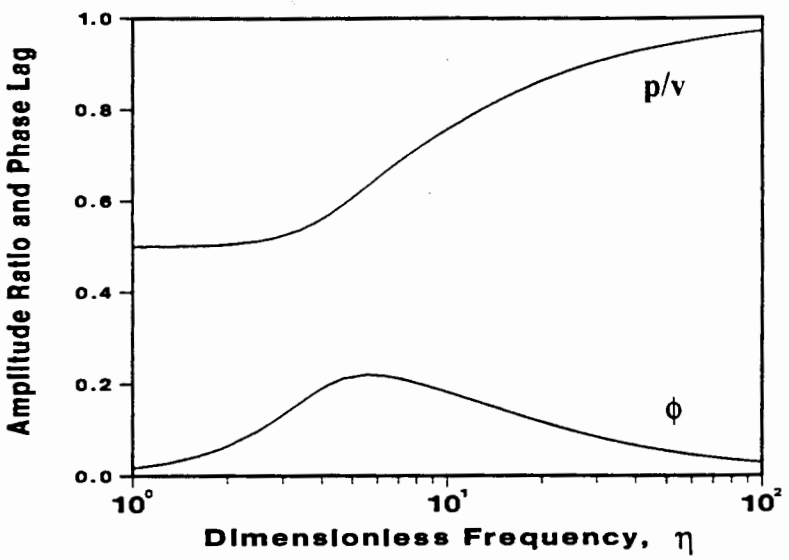
Amplitude Ratio and Phase Lag
1.0
0.8
0.6
0.4
0.2
0.0
p/v
ϕ
10°
10¹
10²
Dimensionless Frequency, η

Figure 4

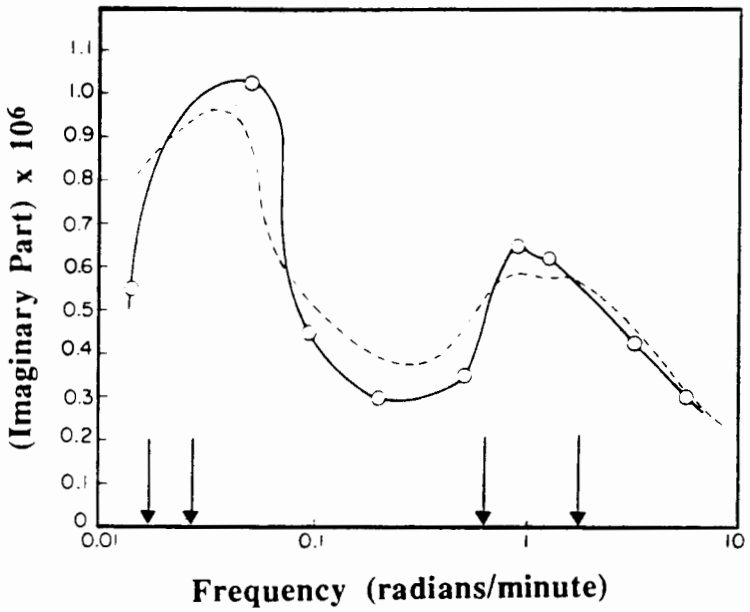
(Imaginary Part) x 10⁶
1.1
1.0
0.9
0.8
0.7
0.6
0.5
0.4
0.3
0.2
0.1
0
0.01
0.1
1
10
Frequency (radians/minute)

Figure 5

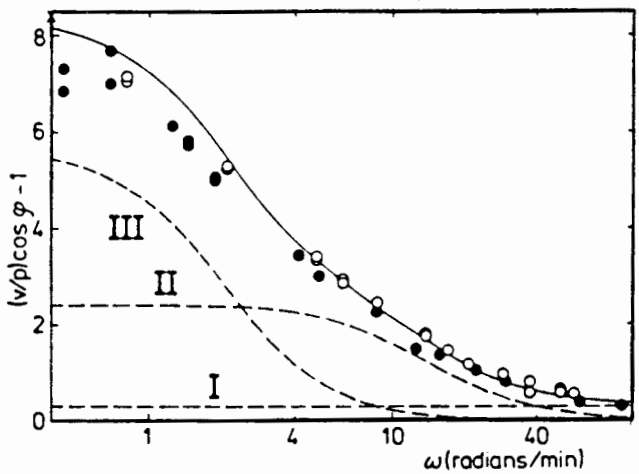

Figure 6

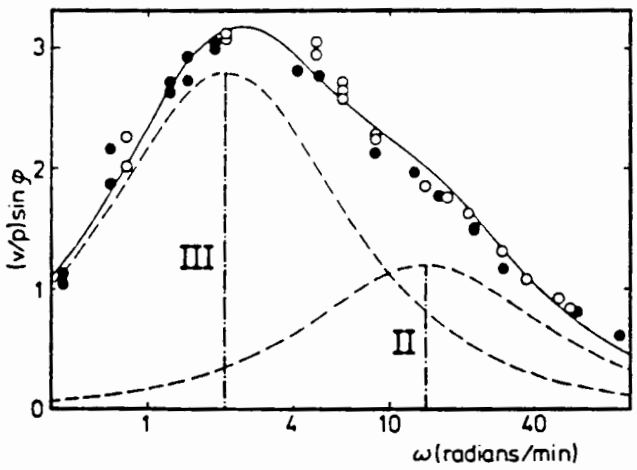

Figure 7

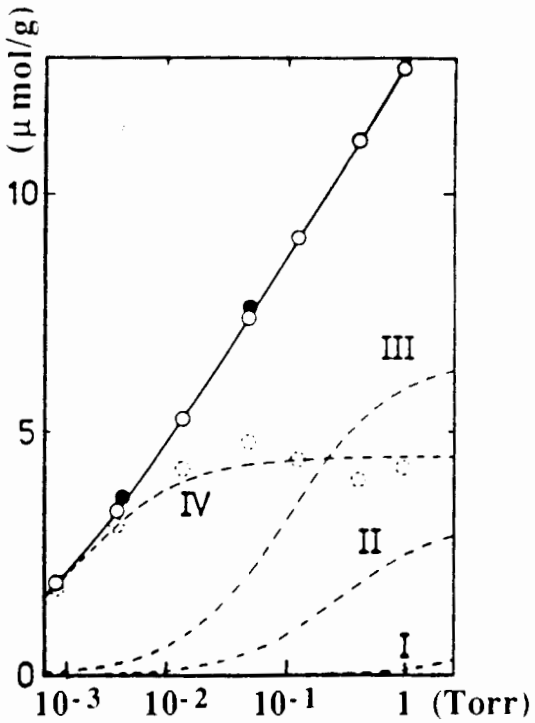

Figure 8

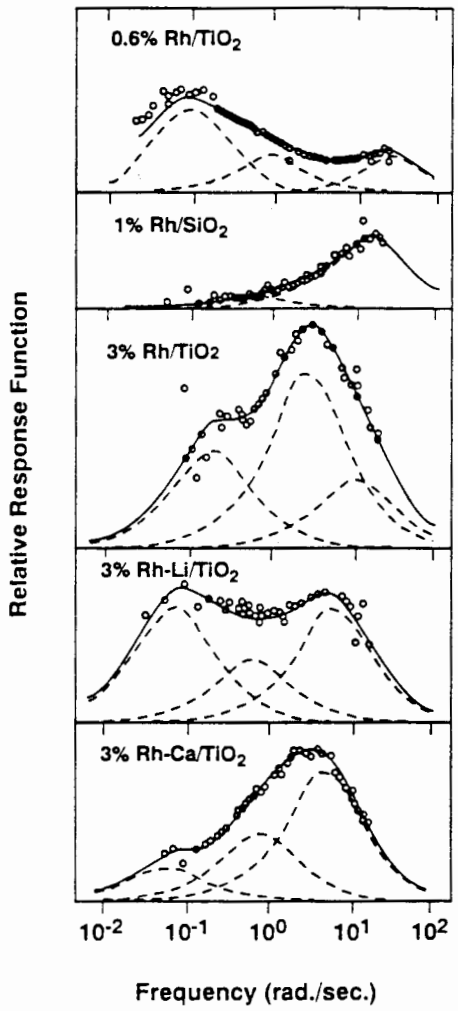
0.6% Rh/TiO2
1% Rh/SiO2
3% Rh/TiO2
3% Rh-Li/TiO2
3% Rh-Ca/TiO2
Relative Response Function
10-2
10-1
100
101
102
Frequency (rad./sec.)

Figure 9

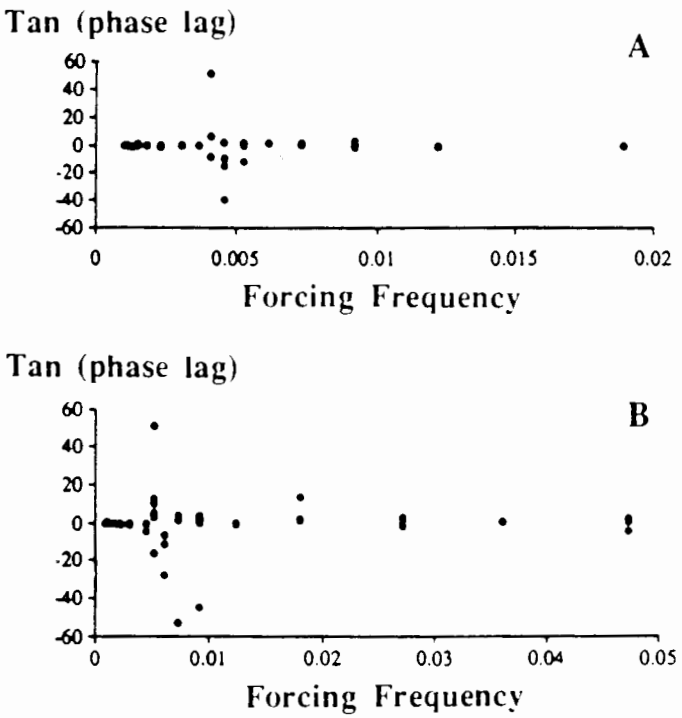
Tan (phase lag)
A
60
40
20
0
-20
-40
-60
0
0.005
0.01
0.015
0.02
Forcing Frequency
Tan (phase lag)
B
60
40
20
0
-20
-40
-60
0
0.01
0.02
0.03
0.04
0.05
Forcing Frequency

Figure 10

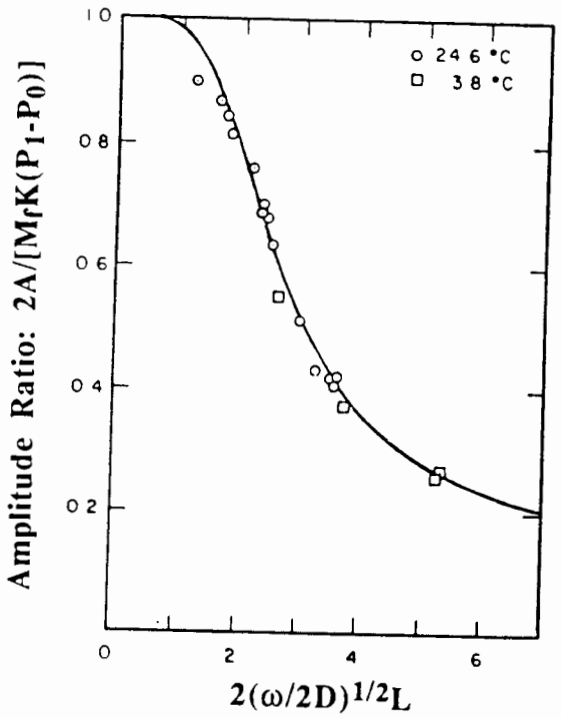
Amplitude Ratio: 2A/[MrK(P1-P0)]
1.0
0.8
0.6
0.4
0.2
0
2
4
6
2(ω/2D)1/2L
24.6 °C
38 °C

Figure 11

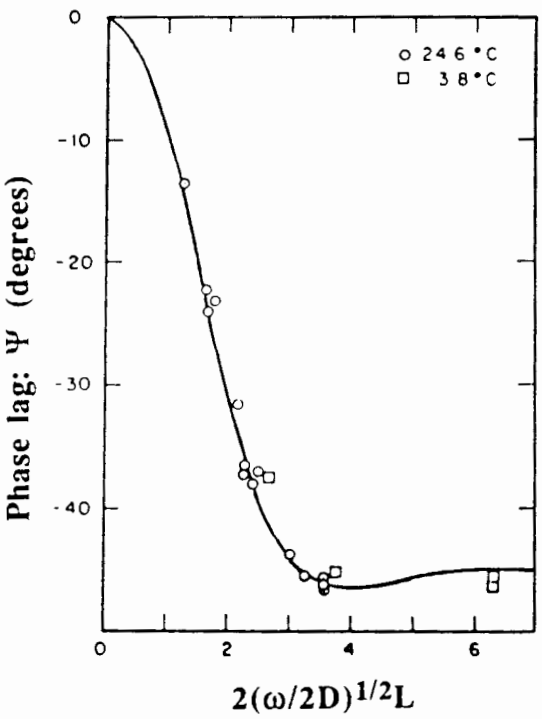

Figure 12

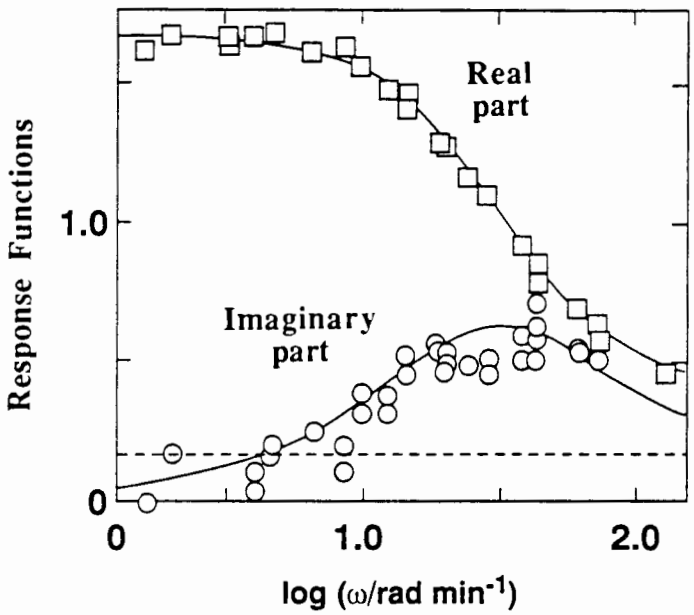
Response Functions
Real part
Imaginary part
1.0
0
0
1.0
2.0
log (ω/rad min-1)

Figure 13

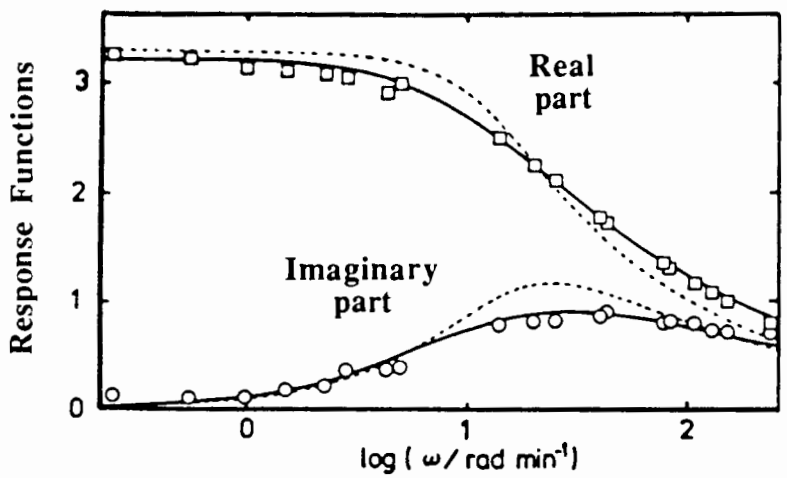
Response Functions
3
2
1
0
Real
part
Imaginary
part
0
1
2
log (ω / rad min⁻¹)

Figure 14

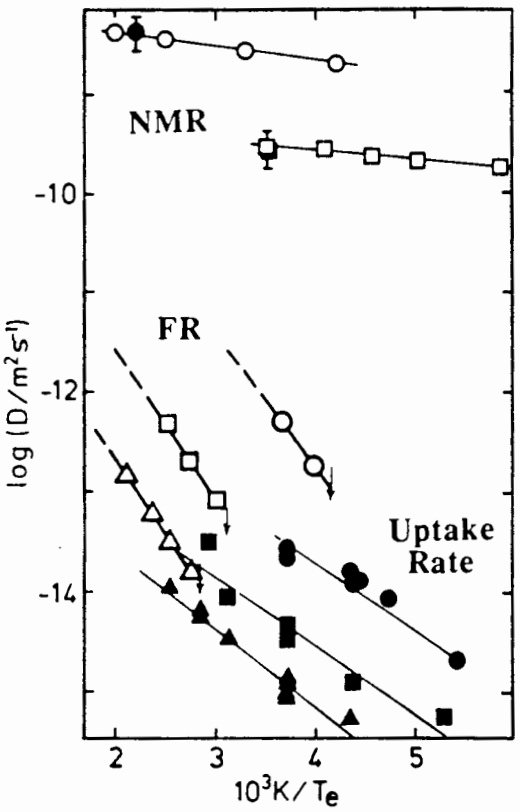

Figure 15

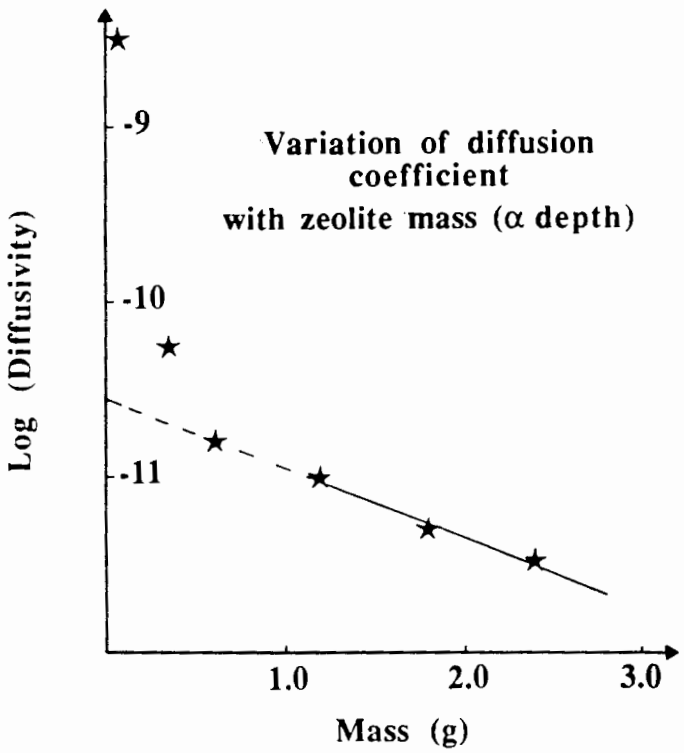
Variation of diffusion coefficient
with zeolite mass (α depth)
Log (Diffusivity)
-9
-10
-11
1.0
2.0
3.0
Mass (g)

Figure 16

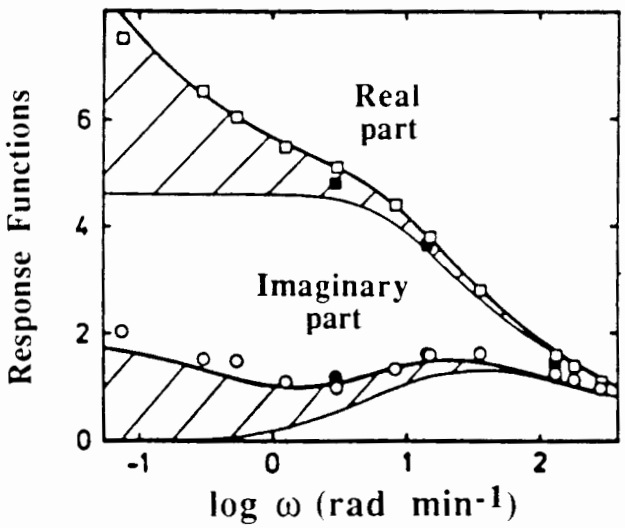
Response Functions
6
4
2
0
Real
part
Imaginary
part
-1
0
1
2
log ω (rad min-1)

Figure 17

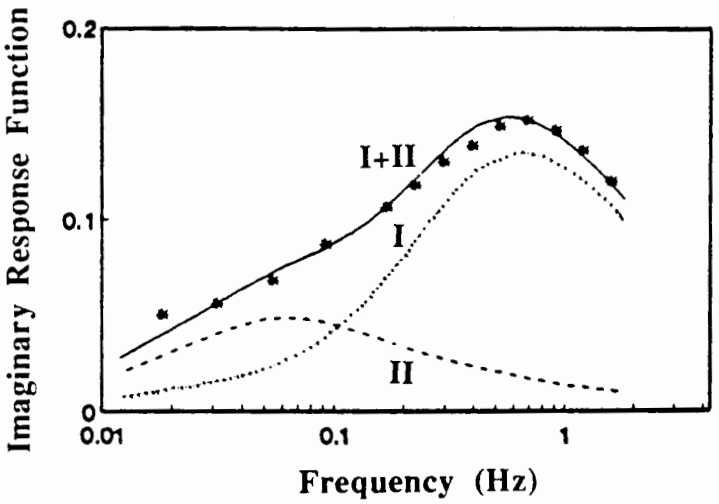
Imaginary Response Function
0.2
0.1
0
0.01
0.1
1
I+II
I
II
Frequency (Hz)

Figure 18

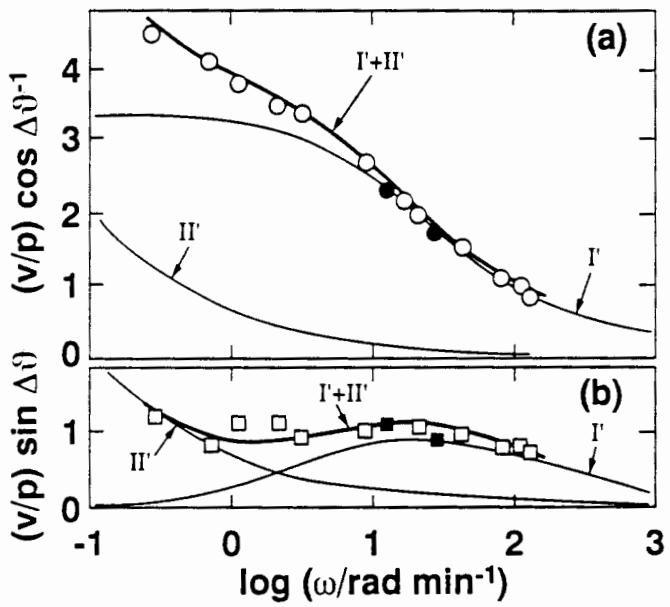
(a)
I'+II'
II'
I'
(b)
I'+II'
II'
I'
(v/p) cos Δϑ-1
(v/p) sin Δϑ
log (ω/rad min-1)
4
3
2
1
0
-1
0
1
2
3

Figure 19

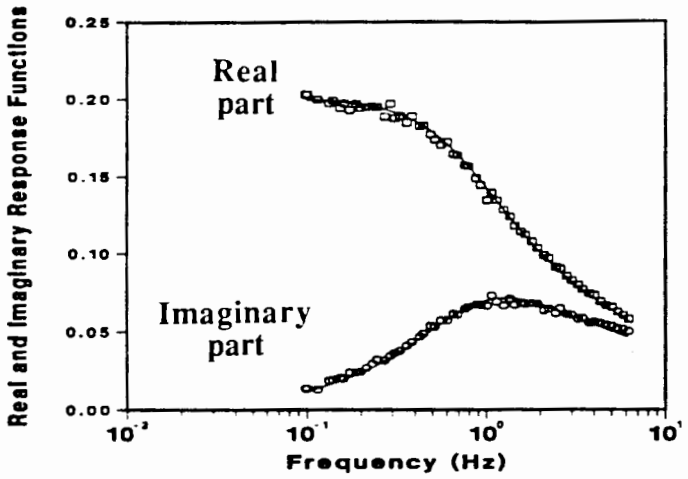
Real and Imaginary Response Functions
0.25
0.20
0.15
0.10
0.05
0.00
Real part
Imaginary part
10⁻²
10⁻¹
10⁰
10¹
Frequency (Hz)

Figure 20

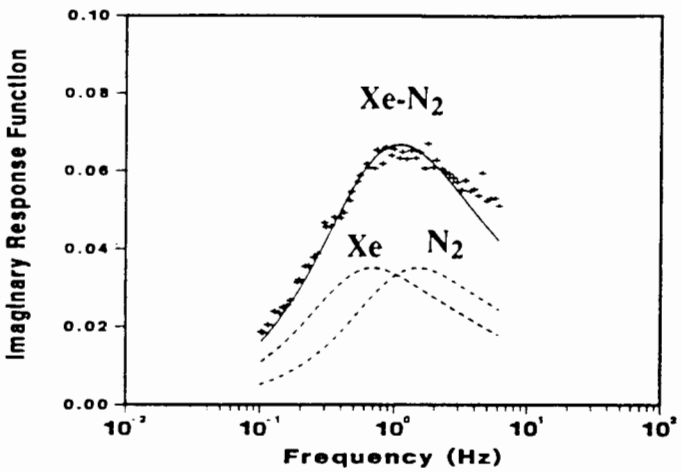
Imaginary Response Function
0.10
0.08
0.06
0.04
0.02
0.00
Xe-N2
Xe
N2
10-2
10-1
100
101
102
Frequency (Hz)

Figure 21

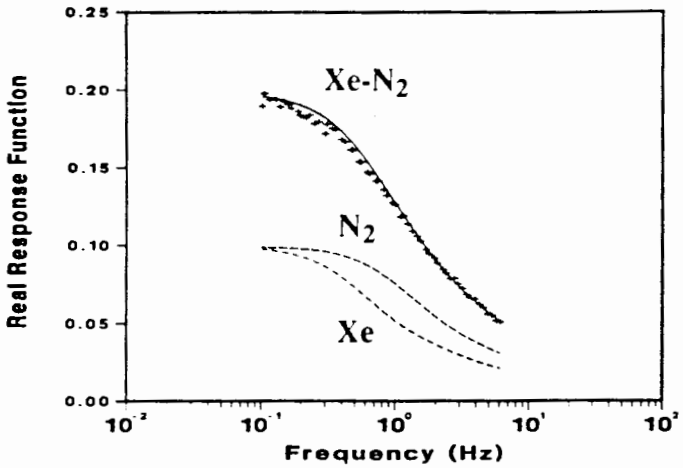
Real Response Function
0.25
0.20
0.15
0.10
0.05
0.00
Xe-N2
N2
Xe
10-2
10-1
100
101
102
Frequency (Hz)

Figure 22

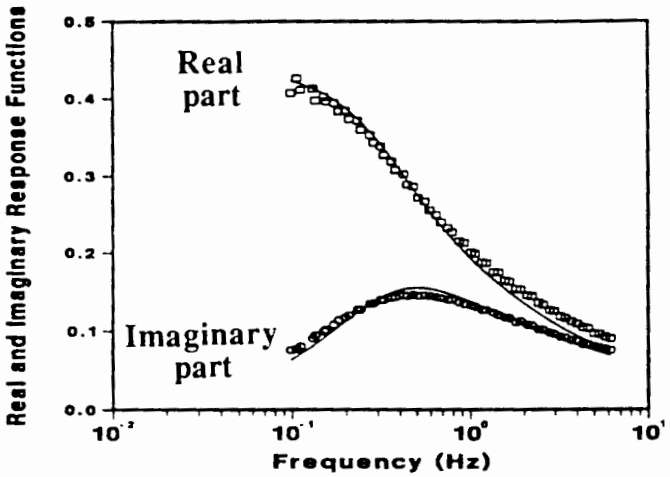
Real and Imaginary Response Functions
0.5
0.4
0.3
0.2
0.1
0.0
Real part
Imaginary part
10⁻²
10⁻¹
10⁰
10¹
Frequency (Hz)

Figure 23